

HIGH TEMPERATURE THICKNESS MONITORING USING ULTRASONIC WAVES

A Thesis
Presented to
The Academic Faculty

by

Joannes C. Pezant

In Partial Fulfillment
of the Requirements for the Degree
Master of Science in Electrical and Computer Engineering in the
School of Electrical and Computer Engineering

Georgia Institute of Technology
December 2008

HIGH TEMPERATURE THICKNESS MONITORING USING ULTRASONIC WAVES

Approved by:

Professor Jennifer E. Michaels, Advisor
School of Electrical and Computer
Engineering
Georgia Institute of Technology

Professor Thomas E. Michaels
School of Electrical and Computer
Engineering
Georgia Institute of Technology

Professor Laurence J. Jacobs
School of Civil and Environmental
Engineering
Georgia Institute of Technology

Date Approved: 13 November 2008

To the girl next door...

ACKNOWLEDGEMENTS

First and foremost, I would like to thank my advisor, Dr. Jennifer Michaels, and her husband and colleague, Dr. Thomas Michaels, who gave me the opportunity to work on this project. The quality of their advice greatly improved my technical as well as organizational skills. I'll never thank them enough for the experience they gave me and also for their forbearance towards my linguistical skills at my arrival.

Dr. Laurence Jacobs, third member of my committee, is an amazing teacher and I really appreciated the conversations I had with him.

I also enjoyed the collaboration with Mechanical Integrity, Inc., and more particularly with Donald McNicol.

I want to thank my labmates for the quiet working environment they provided, and the nice discussions I had with them. I particularly thank James Hall who contributed to improve my English skills as an "interactive dictionary."

I am grateful to Mr. Maheo, the best English teacher I ever had in France, who gave me confidence in my ability to study abroad, even if I had to wait for a complete immersion to make real progress.

I would like to thank my family and friends for their continuous support in my life, and particularly my parents for the wonderful environment in which I grew up.

I also would like to thank the numerous individuals who made my stay in Atlanta more pleasant, particularly Steve, Bryan, Nicolas, Laurent, James, Greg, Helene, Pierrick, Yann, Patrick and Adan.

In addition, my everyday life was greatly improved by my roommates Romain and Sheena, with whom I shared many nice times.

Finally, this work was sponsored by the National Science Foundation under grant

number IIP-0740663 to Mechanical Integrity, Inc., as a part of the NSF STTR program.

TABLE OF CONTENTS

DEDICATION	iii
ACKNOWLEDGEMENTS	iv
LIST OF TABLES	viii
LIST OF FIGURES	ix
SUMMARY	xii
I INTRODUCTION	1
II BACKGROUND	3
2.1 Ultrasonic Thickness Measurements	3
2.1.1 Pulse-Echo Method	3
2.1.2 Pitch-Catch Method	5
2.2 Trailing Echo Generation in Waveguides	6
2.3 Thickness Measurements with a Waveguide	9
2.3.1 Attenuation of Trailing Echoes	9
III STUDY OF WAVE PROPAGATION IN RODS	12
3.1 Overview	12
3.2 Experimental Methods	13
3.3 Simulation Tools	14
3.3.1 Finite Difference Model	15
3.3.2 Ray Tracing Model	16
IV WAVEGUIDE OPTIMIZATION	22
4.1 Rod Dimensioning	22
4.1.1 External Constraints	22
4.1.2 Influence of Rod Diameter on Signals	22
4.1.3 Influence of Rod Length on Signals	24
4.1.4 Discussion and Choice of the Final Dimensions	24

4.2	Impact of the Source on Trailing Echoes	26
4.3	Influence of Boundary Modifications on Trailing Echoes	28
4.3.1	Experimental Observations	31
4.3.2	Results of Simulations	34
4.3.3	Qualitative Analysis of the Results	38
4.3.4	Summary	42
4.4	Imperfect Machining	42
V	WAVEGUIDE IMPLEMENTATION FOR THICKNESS MONITORING	45
5.1	Waveguides and Calibration	45
5.1.1	Calibration Need	45
5.1.2	Dynamic Compensation	48
5.2	Measurement Methods	50
5.2.1	Pulse-Echo Configuration	50
5.2.2	Pitch-Catch Configuration	53
5.3	Final Design	54
5.3.1	Discussion and Choice	54
5.3.2	Concept Validation	55
VI	CONCLUSION	60
6.1	Summary and Conclusions	60
6.2	Future Work	61
	REFERENCES	63

LIST OF TABLES

1	Comparison of the different solutions proposed for trailing echoes attenuation.	11
2	Numerical values associated with the propagation of ray 1.	20
3	Comparison of the experimental and theoretical data available for the time delay between the first arrival and the first trailing echo.	24
4	Error introduced by temperature changes in the measured thickness of a 12.7 mm (1/2") plate	48
5	Impact of the temperature on the measured thickness of a 12.7 mm (1/2") plate after online calibration with the notch echo.	49

LIST OF FIGURES

1	Principle of Pulse-echo measurements.	4
2	Illustration of the time of flight determination for the three modes of ultrasonic thickness measurements (a) Mode 1. (b) Mode 2. (c) Mode 3.	4
3	Principle of pitch-catch measurements.	6
4	Generation of trailing echoes in a cylindrical waveguide.	8
5	Thickness measurements with a waveguide.	10
6	Waveguide modifications for reducing trailing echoes. (a) Grooved rod. (b) Tapered Rod. (c) Clad Rod. (d) Bundle Waveguide.	10
7	Waveform obtained with a cylindrical waveguide of length 152.4 mm (6") and diameter 9.54 mm (3/8") (a) Pulse-Echo Mode. (b) Through-Transmission Mode.	14
8	(a) Geometry used for finite difference simulation of a 0.5 degree tapered rod. (b) Transducer source function.	15
9	Waveform obtained for through-transmission propagation in a cylindrical waveguide of length 152.4 mm (6") and diameter 9.53 mm (3/8"). (a) Simulated with Wave2000. (b) Experimental.	16
10	Wavelet used to model the source emission in the ray tracing model.	17
11	Propagation of a ray in a straight rod	18
12	Contribution of ray 1 to the final waveform.	20
13	Waveforms obtained for the through-transmission in a cylindrical waveguide of length 152.4 mm (6") and diameter 9.53 mm (3/8"), (a) Experimental. (b) Simulated with finite difference. (c) Simulated with ray tracing.	21
14	Comparison of pulse-echo waveforms for rods of same length 101.6 mm (4") and different diameters (a) diameter 9.47 mm (3/8"). (b) diameter 12.64 mm (1/2"). (c) diameter 18.98 mm (3/4").	23
15	Comparison of pulse-echo waveforms for rods of same diameter (3/8") and different lengths (a) length 101.6 mm (4"). (b) length 152.4 mm (6"). (c) length 203.2 mm (8").	25
16	Model of transducer emission.	27

17	Through-transmission waveforms in a cylindrical rod of length 152.4 mm (6") and diameter 9.54 mm (3/8") for several transducer diameters.	29
18	Relative attenuation of the trailing echoes with transducer's diameter.	30
19	Waveforms recorded in different measurement configurations on a 0.75° tapered rod of length 152.4 mm (6") and larger diameter 9.54 mm (3/8"). (a) Through-transmission configuration with source at the small end. (b) Through-transmission configuration with source at the large end. (c) Pulse-echo configuration with source at the small end. (d) Pulse-echo configuration with source at the large end.	31
20	Experimental waveforms for different taper angles on a waveguide of length 152.4 mm (6") and diameter 9.54mm (a) straight rod. (b) 0.25° taper angle. (c) 0.50° taper angle. (d) 0.75° taper angle. (e) 1° taper angle.	32
21	Amplitude of the first trailing echo relative to the first arrival versus taper angle. Each data point represents a separate waveform acquisition.	33
22	Waveforms resulting from finite difference simulations for different taper angles on a waveguide of length 152.4 mm (6") and diameter 9.54 mm (3/8") (a) straight rod. (b) 0.25° taper angle. (c) 0.50° taper angle. (d) 0.75° taper angle. (e) 1° taper angle.	34
23	Impact of the taper angle on the trailing echo attenuation with the finite difference model.	35
24	Waveforms resulting from ray tracing simulations for different taper angles on a waveguide of length 152.4 mm (6") and diameter 9.54mm (3/8") (a) straight rod. (b) 0.25° taper angle. (c) 0.50° taper angle. (d) 0.75° taper angle. (e) 1° taper angle.	36
25	Same as Figure 24 after zooming on the trailing echoes (a) straight rod. (b) 0.25° taper angle. (c) 0.50° taper angle. (d) 0.75° taper angle. (e) 1° taper angle.	37
26	Impact of the taper angle on the trailing echo attenuation with the ray tracing model.	37
27	Comparison of trailing echo amplitude ratios from experiments and both simulations.	38
28	Change in arrival times of trailing echo rays after introduction of a taper angle.	39
29	Variability of the "widening" effect with the trailing echo order. (a) First order trailing echo order. (b) Second order trailing echo.	41

30	Example of imperfect machining.	43
31	Comparison of two tapered rods with different quality of machining. (a) Bad machining. (b) Good machining.	44
32	Comparison of the wave paths corresponding to the backwall echo for the pulse-echo and pitch-catch configurations.	47
33	Replacement of the calibration echo through notch digging. (a) Waveg- uide with a notch. (b) Impact of the notch on the pulse-echo waveform.	49
34	Pulse-echo waveforms in cylindrical waveguides of length 152.4 mm (6") (a) Rod of diameter 9.54 mm (3/8") with a notch of reflective area of 56% ($d_n=3.21$ mm). (b) Rod of diameter 12.7 mm (1/2") with a notch of reflective area of 33% ($d_n=1.73$ mm).	50
35	Pulse-echo measurements with a tapered rod.	51
36	Design of a cylindrical waveguide enabling pulse-echo thickness mea- surements. (a) Random waveguide and its pulse-echo waveform. (b) Optimization of the rod dimensions for the first arrival to be more im- portant than it trailing echoes. (c) Notch dimensioning to minimize the trailing echoes associated with the the calibration echo while increasing the amplitude of the backwall echo.	52
37	Thickness measurement in a pitch-catch configuration with waveguides.	54
38	Experimental setup for concept verification of the pitch-catch measure- ments (a) Picture of the actual setup. (b) Parameters of the experiment.	56
39	Experimental waveforms for pitch-catch measurements. (a) Pulse-echo waveform. (b) Through-transmission waveform.	56
40	Generation of trailing echoes in a cylindrical waveguide.	58
41	Thickness measurements at room temperature.	58
42	Results of thickness measurements at elevated temperatures. The ini- tial calibration was performed at 22.5 °C.	59

SUMMARY

The time required for inspection and maintenance of piping systems and vessels needs to be reduced to both minimize down time and decrease operational costs of petrochemical plants. Current ultrasonic inspection systems are not suited for on-line monitoring, with the main issues being the resistance of transducers and their coupling to high temperatures and the removal of insulation to access structures.

The use of welded cylindrical rods is thus proposed to transfer transducers and their coupling to a lower temperature environment. However, when traveling through waveguides, waves are subjected to numerous mode conversions that result in the creation of new delayed echoes called “trailing echoes.” These echoes can impede measurements and their attenuation needs to be investigated to enable use of waveguides. Among other solutions proposed in the literature, tapered rods are chosen for their good results and their independence from material properties, which makes them good candidates for welding. The impact of the taper angle on trailing echoes is studied through both simulations and experiments. While clean signals can always be obtained by increasing the taper angle in long rods, that is not always the case for short rods, which are considered here.

In addition, temperature variations have a non-negligible impact on the arrival time of the backwall echo when performing measurements with a waveguide, and on-line compensation is essential. Since the interface echo between the rod and the pipe wall may be suppressed after the welding operation, a notch is machined at the end of the rod to create a reflected echo, which can be used for on-line compensation.

Finally, the implementation of waveguides is considered for both pulse-echo and

pitch-catch modes. In the pitch-catch mode, the backwall echo and the notch echo are received by different transducers and signals of interest are both first arrivals. As a result, trailing echoes do not impede measurements and their attenuation becomes unnecessary. In contrast, pulse-echo measurements are sensitive to trailing echoes and the waveguide's design plays an essential role in the feasibility of measurements. However, the environment also imposes a set of constraints on waveguide dimensions that complicates the implementation of pulse-echo measurements. Being more flexible, the pitch-catch configuration is chosen for final implementation. Experiments are performed to verify the concept feasibility, and the accuracy of measurements with thickness and temperature changes is also confirmed.

The major contributions of this thesis are the development of a 2D ray tracing model to enable a better understanding of wave propagation in short tapered rods, the understanding of the taper angle influence on trailing echoes in short rods, and the development and comparison of potential solutions for high temperature thickness monitoring.

CHAPTER I

INTRODUCTION

The American Petroleum Institute has reported that almost every unplanned refinery shutdown is linked to failures of piping systems [1]. The negative effects of such incidents are amplified by the difficulty of maintenance personnel to anticipate needed repairs. The development of on-line monitoring systems for pressure vessels and piping systems could thus play a critical role in the minimization of both plant down time and maintenance expenses.

Existing nondestructive inspection methods based on wave propagation are in common usage for measuring the wall thickness of pipes and pressure vessels [2, 3]. These methods are suitable for periodic inspection, either manually or with automated scanning equipment. More recently, the trend is towards the implementation of permanently mounted monitoring systems able to provide near real-time data [4].

The failure of piping systems is caused by corrosion and erosion that result in wall thinning. As of today, the integrity of pipelines is verified through a time and cost intensive inspection process. Production is stopped, the insulation is removed, and transducers are mounted directly on pipe walls for thickness measurements [5].

Each time an inspection is performed, the productivity of the plant is reduced, resulting in a significant loss of money. The use of an on-line monitoring system could minimize these losses by allowing measurements with minimal effect on production. Additionally, it would reduce the testing personnel since the insulation would not need to be removed, and it would give faster results. However, the average operating temperature of pipe walls is around 500°C, which introduces issues of transducer survivability and coupling longevity.

As a result, traditional inspection methods have to be adapted to enable thickness measurements at high temperature. After a review of existing literature on high temperature thickness measurements, this thesis proposes new solutions to enable on-line monitoring of pipe walls based upon the use of welded waveguides to solve the issue of transducer coupling and survivability at high temperature. Several configurations for the implementation of welded waveguides are presented, and the most appropriate are selected for the specific application of pipeline monitoring. Finally, results are provided to prove the concept feasibility.

CHAPTER II

BACKGROUND

This background summary presents prior technical knowledge relevant to this study. After a review of the basics of ultrasonic thickness measurements, the generation of “trailing echoes” in waveguides is presented and means of minimizing them are explained.

2.1 Ultrasonic Thickness Measurements

Ultrasonic thickness measurements are performed by transducers emitting waves in the tested structure. There are different methods for measurements, but they are all based on the wave’s time-of-flight through the structure. The first method is called “pulse-echo” and requires only one transducer. The second method, called “pitch-catch,” requires two transducers located in close proximity. In this study, the material is considered to be homogeneous as is the customary assumption.

2.1.1 Pulse-Echo Method

In pulse-echo measurements, a transducer emits waves through the measured specimen and the echoes reflected back are analyzed for thickness determination [6]. The experimental setup for measuring the thickness of a plate is presented in Figure 1. The wave’s time-of-flight for a round-trip through the plate is proportional to the thickness of the plate,

$$d = c \frac{\Delta t}{2}, \tag{1}$$

where d is the thickness of the plate, c the wave velocity through the plate, and Δt the time needed for a round-trip through the plate.

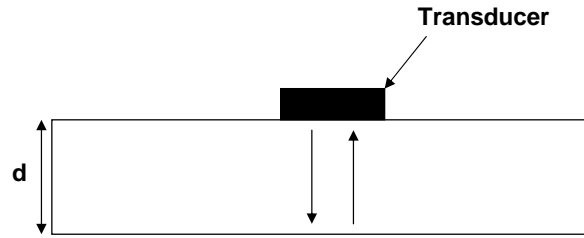


Figure 1: Principle of Pulse-echo measurements.

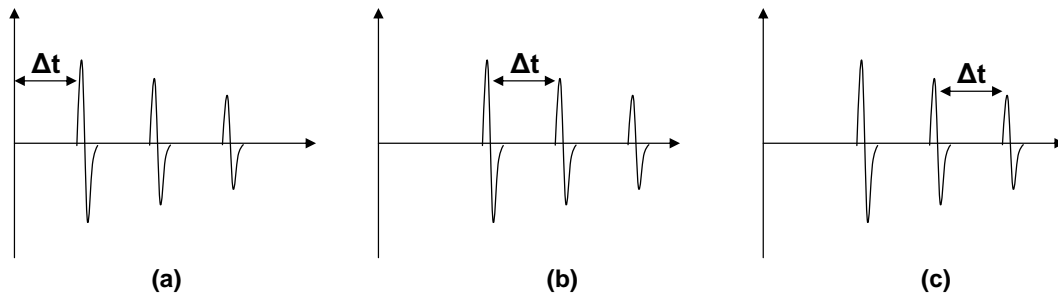


Figure 2: Illustration of the time of flight determination for the three modes of ultrasonic thickness measurements (a) Mode 1. (b) Mode 2. (c) Mode 3.

There are three different measurement modes depending on the echoes considered for the time-of-flight determination as shown in Figure 2 [6]. If calculation is based on the first backwall echo only, the measurement is said to be a “mode 1”. It may not be the most accurate mode due to variability in the coupling layer, and is used when a front echo is not available, such as is the case for contact transducers.

For immersion or delay line transducers, the time-of-flight corresponds to the time delay between the echo resulting from reflection on the front surface of the plate and the echo reflected from the back surface. This measurement is called a “mode 2” and is generally more precise than a mode 1.

Finally, a third mode exists that can apply to any kind of transducer. Once inside the plate, waves bounce between the two boundaries, creating a series of echoes with a constant time interval corresponding to a round-trip in the plate. Thus, the time-of-flight can be measured as the time delay between two sequential echoes. This method,

referred to as “mode 3”, is the most accurate since it uses two echoes subjected to the same uncertainties and many errors are cancelled. However, it requires at least two echoes of sufficient amplitude, which are not always available.

As a result, measurements are performed in mode 3 as long as suitable echoes are available. Otherwise, mode 1 or mode 2 is considered depending on the experimental setup.

Regardless of the mode type, the velocity in Eq.(1) is typically determined via a calibration process whereby times are measured from samples of known thicknesses and material of interest. A time offset is usually required, particularly if there is a phase reversal between echoes; i.e.

$$d = c \frac{(\Delta t - t_{off})}{2} \quad (2)$$

where t_{off} is the time offset. The unknown parameters c and t_{off} are determined via linear regression.

In more complex structures, additional echoes might appear, making the echo identification more difficult. However, the principles are still the same.

2.1.2 Pitch-Catch Method

Though many thickness measurements are performed in a pulse-echo configuration, there exists an alternative method called “pitch-catch” that uses a separate transmitter and receiver. Measurements can be performed either with a dual element transducer [7] or with two separate transducers. This method presents several advantages depending on the context. For example, it is a very interesting solution in curved plates where waves are not necessarily reflected directly back to the transmitter.

In this configuration, the time-of-flight of the waves traveling between the transmitter and the receiver does not exactly correspond to a round-trip through the plate because the waves are not propagating at normal incidence. Calibration is needed

and the thickness can be determined by,

$$d = a_0 + a_1 \Delta t, \quad (3)$$

where d is the thickness of the plate, Δt is the time needed for the wave to travel between the transmitter and the receiver, and a_0 and a_1 are calibration constants obtained experimentally with several measurements at different known thicknesses. This calibration is essentially the same as that of Eq.(2), although the interpretation of the constants is somewhat different.

There is only one measurement mode for the pitch-catch method, mode1, which is based on the arrival time of the first echo reaching the receiver. Figure 3 illustrates pitch-catch measurements.

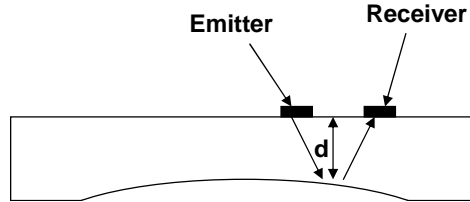


Figure 3: Principle of pitch-catch measurements.

2.2 *Trailing Echo Generation in Waveguides*

In the context of high temperature measurements, the use of cylindrical waveguides with the transducer mounted to one end and the other end contacting the part is often considered. The primary purpose of the waveguide is to prevent the transducer from directly contacting the hot part. Use of a cylindrical waveguide requires understanding of waves propagation in circular rods. The first study of wave propagation in circular rods dates from 1876 and was proposed by Pochhammer as mentioned in the classic book by [8]. However, this study was limited to longitudinal waves. The

extension to shear waves was proposed in 1956 by McSkimin [9]. In between, Mason observed in 1947 that the reduction of the rod diameter brought new undesired echoes that are now commonly referred to as trailing echoes [10]. Since then, waveguides have been extensively used for high-temperature measurements [11] [12]. However, trailing echoes can have a significant impact on measurements, and it is necessary to understand their origin to manage them and avoid problems when performing thickness measurements.

Here we are interested in the regime where the wavelength is much less than the diameter of the rod, meaning that the wave propagation can be thought of in terms of bulk waves interacting with boundaries. Each time a wave reflects from a boundary, there can be two reflected waves, one longitudinal and one shear, of different amplitudes, angles and wave speeds. In a waveguide, the proximity of boundaries increases the number of mode conversions. As a result, a wave emitted by the transducer splits into several sub-waves propagating independently.

The difference between the arrival times of two sub-waves is essentially related to distances traveled as longitudinal and shear waves. In a cylindrical waveguide, the possible distances traveled as a shear wave are quantified and are roughly proportional to the number of mode conversions to which the wave is subjected. As a result, the arrival times of the sub-waves are grouped around specific times related to the number of mode conversions. The sub-waves constructively interfere and create undesired echoes called trailing echoes.

Figure 4 illustrates the trailing echoes generated for one-way propagation in a cylindrical rod. Points 1 and 2 are typical points of the transmitter.

In reality, waves have a grazing incidence on boundaries and the angle α is much smaller than the representation given in Figure 4. As a result, variations in α have a very impact on the arrival times of the sub-waves, which just depend on the number

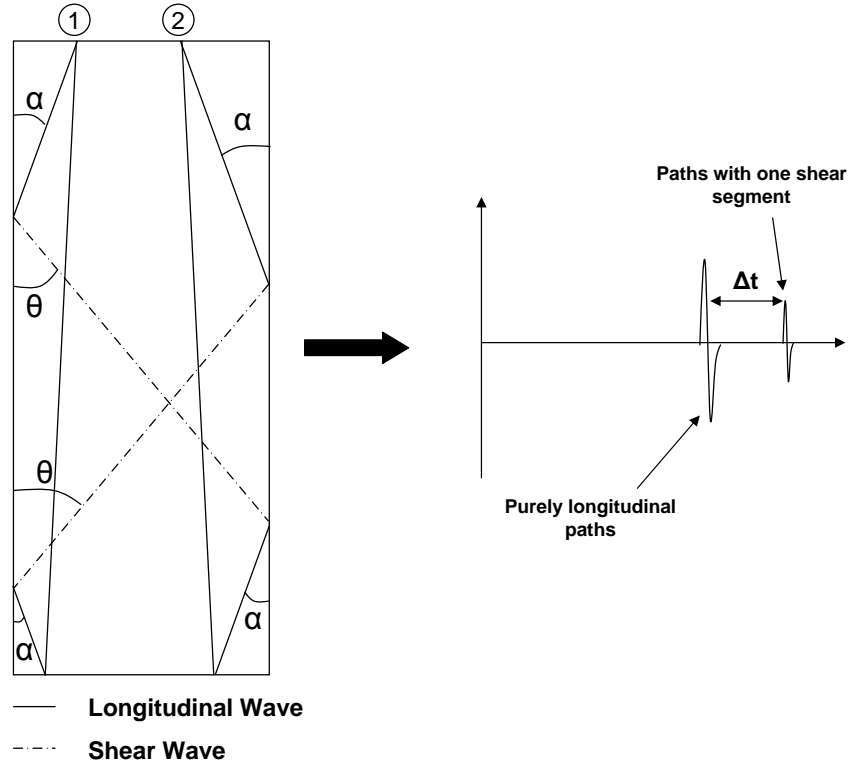


Figure 4: Generation of trailing echoes in a cylindrical waveguide.

of mode conversions they are subjected to. This results in the creation of new delayed echoes corresponding to different numbers of mode conversions, called trailing echoes.

The time delay between the first arrival and the first trailing echo is the same as the time delay between two consecutive trailing echoes, and can be calculated theoretically by the limiting case when α equals zero [13],

$$\Delta t = \frac{d}{c_T \cos(90 - \theta)} - d \frac{\tan(90 - \theta)}{c_L} = \frac{d}{\tan(\theta)} \times \frac{c_L^2 - c_T^2}{c_L c_T^2}. \quad (4)$$

Here d is the thickness of the plate, Δt is the time delay between two trailing echoes, c_L and c_T are the respective longitudinal and shear wave velocities, and θ is the complement of the refracted angle of the shear wave shown in Figure 4 and obtained via,

$$\theta = 90 - \sin^{-1}\left(\frac{c_T}{c_L}\right). \quad (5)$$

Note that in the case when an echo arriving after the first arrival is needed for a thickness measurement, it can be obscured by the trailing echoes, making thickness measurements inaccurate or impossible. In addition, the time delay between each echo is proportional to the diameter of the rod. As a result, the smaller the diameter of the rod, the greater the affect on thickness measurements.

2.3 Thickness Measurements with a Waveguide

Even though several methods exist for thickness measurements, they are all based on the same idea. The time-of-flight through the inspected specimen is measured and the wave velocity is then used to calculate the thickness. When a waveguide is used, waves propagate through it before entering the specimen and every echo is delayed.

In the context of high temperature measurements, a temperature gradient is expected in the rods. This gradient may vary because the temperatures at its ends can change. If there is no interface echo between the rod and the part, such as might be the case when there is excellent coupling and no impedance mismatch, only a mode 1 measurement is possible. However, the temperature-induced velocity changes are generally too large for this approach to have the needed accuracy. The common approach consists in requiring that an echo exists from the interface between the rod and the specimen so that a mode 2 measurement can be made. Specifically, the arrival time of the reflected echo is subtracted from the arrival time of the backwall echo to deduce the time-of-flight through the specimen, and the assumption is made that the velocity in the specimen is constant.

2.3.1 Attenuation of Trailing Echoes

The interface echo and the backwall echo are both followed by their trailing echoes. As a result, the trailing echoes associated with the interface echo can hide the backwall echo, making any thickness measurement impossible. To avoid this situation, several methods have been proposed to attenuate the trailing echoes. These are illustrated

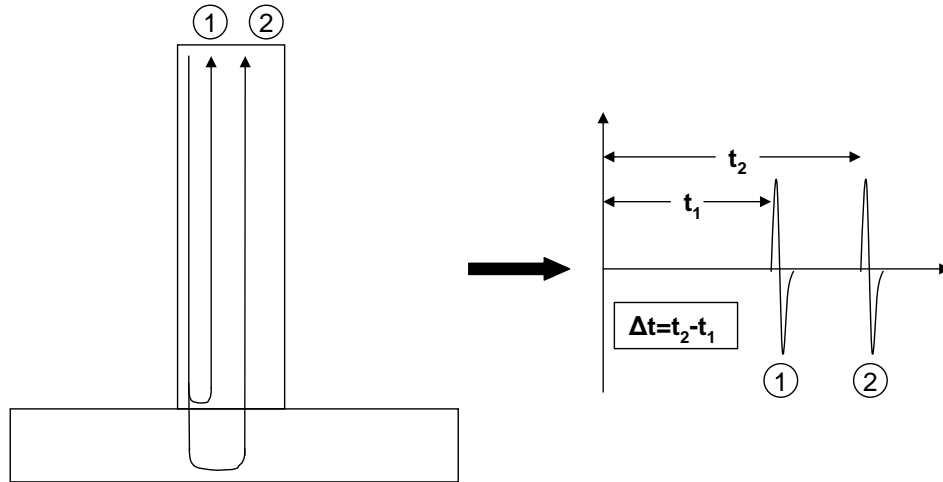


Figure 5: Thickness measurements with a waveguide.

in Figure 6.

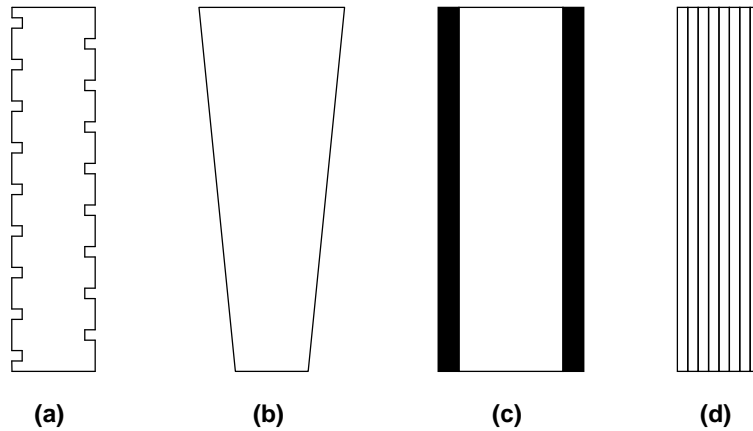


Figure 6: Waveguide modifications for reducing trailing echoes. (a) Grooved rod. (b) Tapered Rod. (c) Clad Rod. (d) Bundle Waveguide.

Most of the solutions lie in the modification of the boundaries since trailing echoes are generated via mode conversions at the rod boundaries. The first one consists in using grooved rods and was first considered in 1959 by McSkimin [14]. This proved to attenuate trailing echoes, but it did not suppress them completely. The use of tapered rods was first considered in 1990 [15]. They were shown to attenuate trailing

echoes, but reduced the energy transmitted to the specimen. In parallel, clad rods were investigated and proved to provide very good attenuation of trailing echoes [16]. They are widely used today for measurements and sometimes combined with rod tapering for optimal results [17] [18].

Besides boundary modifications, the use of bundle waveguides was considered [19]. The underlying idea is that trailing echoes are not generated in waveguides of diameter smaller than a wavelength. However, tiny waveguides do not provide a sufficient signal-to-noise ratio for thickness measurements. It is thus necessary to use several of them packed tightly together to perform measurements. This solution is potentially interesting, but the attachment of the bundle waveguides to both the transducer and part is problematic, which reduces its practicality.

Table 1: Comparison of the different solutions proposed for trailing echoes attenuation.

Solution	Strengths	Weaknesses
Grooved Rod	Inexpensive and easy to machine	Limited signal improvements
Tapered Rod	Good results in any material	Reduction in signal-to-noise ratio
Clad Rod	Best signal improvement	Expensive and material dependant
Bundle Waveguide	No trailing echoes	Difficult attachment

CHAPTER III

STUDY OF WAVE PROPAGATION IN RODS

This chapter proposes an approach for the study of high temperature measurements and presents the tools used to accomplish it.

3.1 Overview

Though robust methods exist for ultrasonic thickness measurements, they are not designed for continuous monitoring in high temperature environments. The survival of the transducer and its coupling become major issues when the temperature increases. As a result, methods have to be adapted to support the high temperature environment.

The transducer can be protected from high-temperatures in different ways, but the solution chosen has to allow for reliable coupling. The first option consists in using high temperature transducers, which have a resistance to temperature up to 482 °C [20]. Another solution consists in cooling the transducer with a cooling system [21]. Finally, the background section suggested the use of waveguides as a solution to keep transducers at a reasonable temperature.

Experiments performed by Mechanical Integrity, Inc. showed that a wide variety of coupling methods did not last longer than a few months at high temperatures [22]. Lowering the operational temperature of the couplant is thus necessary to enable long-term measurements. Given the thermal inertia of pipes, it is not possible to cool their walls locally and the only solution consists in transferring the coupling area to a cooler environment. In this perspective, the use of waveguides appears to be the best solution since they can be welded on pipe walls. Then, the transducer and its coupling can be transferred through the insulation to a lower temperature environment (i.e.

the opposite end of the buffer rod) and both issues are addressed simultaneously.

As a result, the decision was made to study the implementation of welded waveguides as a solution to the problem of high temperature measurements. The issue then becomes the management of trailing echoes, which can interfere with echoes of interest and make thickness measurements impossible, as mentioned in the background chapter.

It is thus necessary to address the generation of trailing echoes and their management to allow thickness measurements with buffer rods. In this perspective, both experiments and simulations are performed.

3.2 Experimental Methods

For experiments, plate sections are used instead of pipes, which are a good approximation since the radius of pipes is much bigger than the dimensions of the measurement area. Three steel plates of respective thickness 9.54 mm (3/8"), 12.7 mm (1/2") and 19.05 mm (3/4") were used for the measurements. The waveguides were machined from steel rods of diameter 9.54 mm (3/8"), 12.7 mm (1/2") and 19.05 mm (3/4"). Rods of different lengths and taper angle were machined for experiments in this study.

Testing itself was performed with 10 MHz Panametrics transducers, model V552-SM and diameter 9.54mm (3/8"), excited by a Panametrics pulser-receiver, model 5072 PR. Transducers were coupled to the tested parts with Panametrics couplant A or C. Waveforms were acquired by a Tektronix TDS5034B digital oscilloscope with a sampling frequency of either 125 MHz or 250MHz, and were saved for further analysis.

The pulser-receiver has two measurement modes. In pulse-echo mode, only one transducer is used and it serves as both transmitter and receiver. In through-transmission mode, the transmitter and the receiver are distinct transducers. Figure 7 presents signals obtained in each of these two modes. For pulse-echo mode, a single transducer was mounted on one end of the rod, and for through-transmission mode,

the two transducers were mounted on opposite ends of the rod.

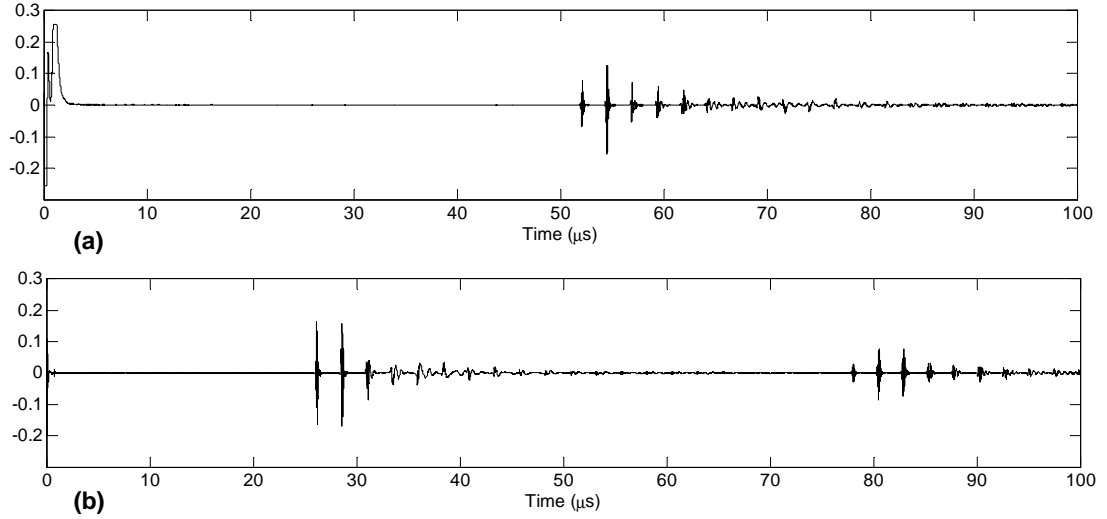


Figure 7: Waveform obtained with a cylindrical waveguide of length 152.4 mm (6") and diameter 9.54 mm (3/8") (a) Pulse-Echo Mode. (b) Through-Transmission Mode.

For better coupling, threaded holders were fabricated to hold the transducers to rods of diameter 9.54 mm (3/8") and 12.7 mm (1/2"). Plastic holders were also fabricated to hold rods at a fixed angle to the plate surface.

3.3 *Simulation Tools*

Simulation tools enable a deeper exploration of wave propagation phenomena while providing more repeatable results than experiments. In addition they reduce the cost of experiments by enabling pre-selection of relevant designs. However, it is important to keep in mind that simulations are approximations and they need to be confirmed by experiments. The simulations reported here are limited to 2D models for simplification and reduction of the computational time. This approximation has to be kept in mind when interpreting the simulation results.

3.3.1 Finite Difference Model

The first model considered for simulations is based on the finite difference method. A commercial software package, Wave2000 [23], was purchased. To permit use of this software, the geometry of the waveguide was represented using a two-dimensional shape. An example is shown in Figure 8, which is the radial-axial cross-section of a tapered waveguide. The source for all Wave2000 simulations was modeled as a 10 MHz sinusoid over two cycles with the built-in source modeling tool. Although it is slightly different from a real tone burst, the main goal of this tool is not to produce a perfect match with the experimental waveforms, but rather to understand the propagation in waveguides to better design them.

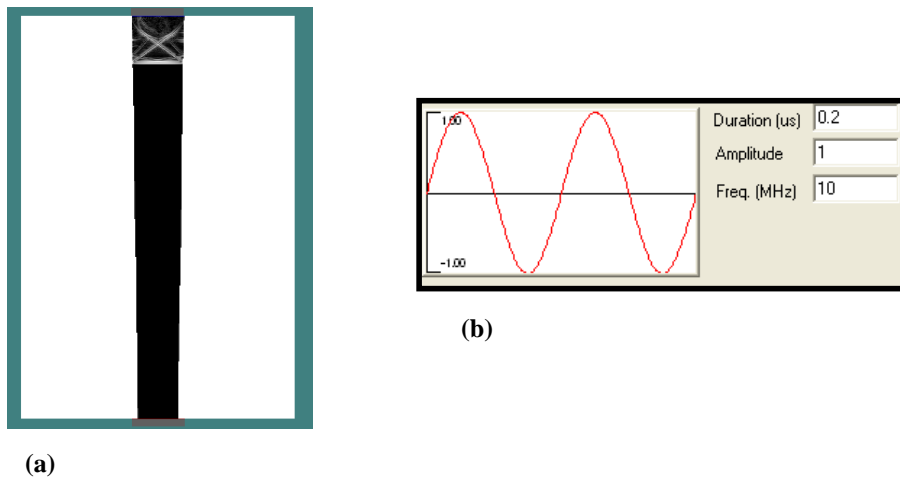


Figure 8: (a) Geometry used for finite difference simulation of a 0.5 degree tapered rod. (b) Transducer source function.

Once the source and the geometry are defined, the software performs finite difference calculations from the transmitter to the receiver to generate the output waveform. The waveform obtained after propagation in a cylindrical waveguide in a through-transmission configuration is provided in Figure 9 as an example. The echo amplitudes do not match the experimental waveform, but the model does capture the trailing echoes. Also the effect of a finite grid appears to introduce noise in the

simulated waveform, as is evident in Figure 9(a).

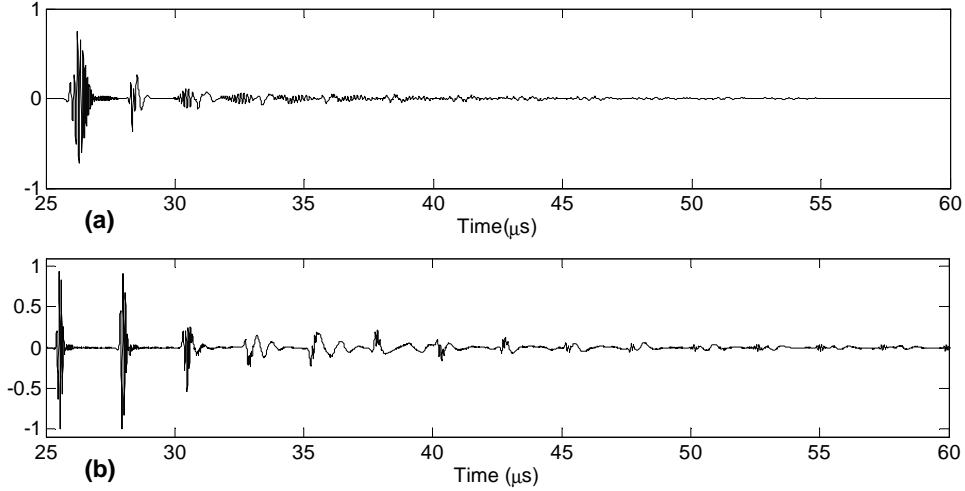


Figure 9: Waveform obtained for through-transmission propagation in a cylindrical waveguide of length 152.4 mm (6”) and diameter 9.53 mm (3/8”). (a) Simulated with Wave2000. (b) Experimental.

3.3.2 Ray Tracing Model

Ray tracing is a geometrical method based on paths of rays emanating from the source [24]. Specifically, the transmitter is modeled as an array of point sources distributed uniformly across its surface, with each point source emitting energy distributed uniformly in angle. Then the path of each ray is computed between the source and the receiver, and the output waveform is generated by adding the contribution of all the rays reaching the receiver. In this approach, there is grid for computation; the points of reflection on the boundaries are determined mathematically without any grid effect at the edges. Thus, there is no numerical noise as was the case for finite difference simulations. The mode conversions on boundaries are taken into account to reproduce the trailing echoes.

The same 2D cross section as the one used for finite differences was used for the 2D representation of the rod. A 3D correction was made by weighting the contribution

from each point source by the annular area corresponding to its radius.

Each point source radiates isotropically in all directions within the 2D cross-sectional plane, and rays were generated every 0.05 degree for the subsequent calculations. Note that rod curvature effects are not taken into account in this model because point sources only emit in the 2D cross-section considered.

Since all the rays emit simultaneously in time at the source, and because material dispersion and attenuation are neglected, the source waveform can be scaled, shifted and added at the receiver based upon the computed arrival time and amplitude of each ray. The arrival time is determined from the path calculation by using the appropriate wave velocity for each propagating mode. The amplitude is updated at each mode conversion using theoretical coefficients for plane wave reflection at a planar boundary [25]. Once this information is gathered for each ray, the received waveform can be generated. For the model to be consistent with experiments, the source waveform was chosen to be a 10 MHz sinusoid multiplied by a Hanning window over three cycles, and is illustrated in Figure 10.

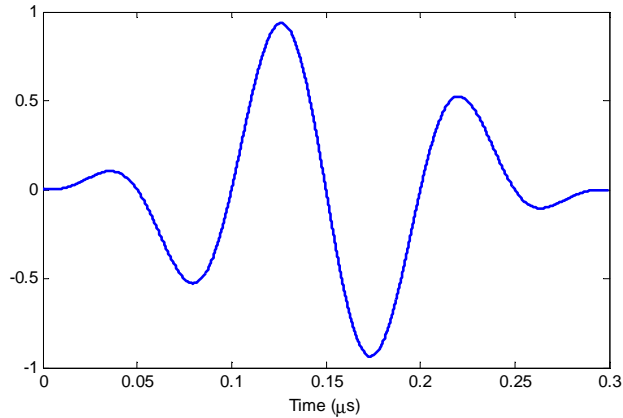


Figure 10: Wavelet used to model the source emission in the ray tracing model.

As an example, the evolution of a ray from its emission to its arrival at the receiver is detailed here and illustrated in Figure 11. Ray 1 is subjected to a mode conversion and splits into rays 2 and 3. Then, ray 2 directly reaches the receiver while ray 3

is subjected to another mode conversion, resulting in rays 4 and 5, both hitting the receiver.

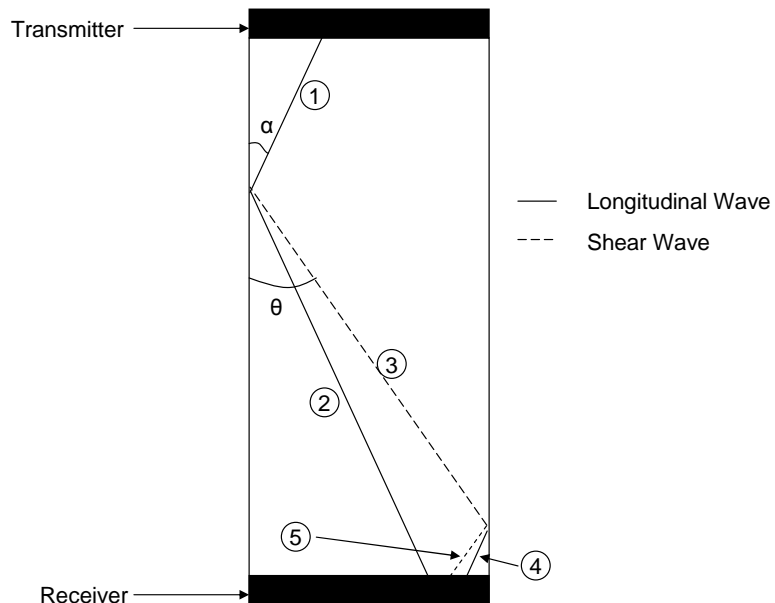


Figure 11: Propagation of a ray in a straight rod

As a result, ray 1 produces three arrivals at the receiver. However, ray 5 reaches the receiver as a shear wave and is thus discarded; the assumption is made that the receiver is only sensitive to longitudinal waves. To create the waveform at the receiver, it is then needed to determine the arrival times and amplitudes of rays 2 and 4.

According to Snell's law, rays 1 and 4 propagate with the same angle α , ray 2 propagates at an angle of $(\pi - \alpha)$, ray 3 propagates at an angle of θ , and ray 5 propagates at an angle of $(\pi - \theta)$. All angles are measured counterclockwise from a vertical line, and α and θ are related by,

$$\theta = \sin^{-1}\left(\frac{c_T}{c_L}\sin\alpha\right), \quad (6)$$

where c_L and c_T are the longitudinal and shear wave respective velocities. The arrival

times are calculated from the ray paths. The first arrival corresponds to the combination of ray 1 and ray 2. The propagation is longitudinal along the entire path, and the arrival time is given by,

$$t_2 = \frac{l_1 + l_2}{c_L}, \quad (7)$$

where l_1 is the length of ray 1, l_2 is the length of ray 2, and c_L is the longitudinal speed of waves in steel. Concerning its amplitude, ray 2 results from the reflection of ray 1 on the boundary. The reflection coefficient is,

$$A_2 = A_1 \times \frac{\sin(2\alpha)\sin(2\theta) - \nu^2\cos^2(2\theta)}{\sin(2\alpha)\sin(2\theta) + \nu^2\cos^2(2\theta)} \quad (8)$$

where ν is Poisson's ratio, A_1 is the amplitude of ray 1, and A_2 the amplitude of ray 2. The second arrival corresponds to the combination of rays 1, 3 and 4. The propagation is longitudinal for rays 1 and 4, and shear for ray 3. Consequently, the arrival time of ray 4 is

$$t_4 = \frac{l_1 + l_4}{c_L} + \frac{l_3}{c_T}, \quad (9)$$

where l_1 is the length of ray 1, l_3 is the length of ray 3, l_4 is the length of ray 4, c_L is the longitudinal wave velocity in steel, and c_T is the shear wave velocity in steel. Finally, the amplitude of ray 4 is determined by considering the amplitude partition resulting from the two mode conversions along its path. The relation between the amplitude of ray 1 and the amplitude of ray 4 is given by,

$$A_4 = -A_1 \times \frac{2\nu^2\sin(4\theta)\sin(2\alpha)\cos(2\theta)}{(\sin(2\alpha)\sin(2\theta) + \nu^2\cos^2(2\theta))^2}, \quad (10)$$

where ν is Poisson's ratio, A_1 is the amplitude of ray 1, and A_4 the amplitude of ray 4.

The contributions of ray 1 to the final waveform can then be plotted by adding

scaled wavelets at the corresponding arrival times. Figure 12 presents the contribution of ray 1, while Figure 13 gives the final waveform obtained via the entire ray tracing simulation. Both figures are for the through transmission in a cylindrical waveguide of length 152.4 mm (6") and diameter 9.54 mm (3/8").

As it was the case for the Wave 2000 simulations, the amplitude partition between the initial and trailing echoes for ray tracing does not match the experiments. However, ray tracing does not have simulation noise resulting from the finite difference grid.

Table 2: Numerical values associated with the propagation of ray 1.

α	θ	Rod Length	Rod Diameter	A_1	A_2	A_4
2°	56.54°	152.4 mm	9.54 mm	1	-0.79	-0.38

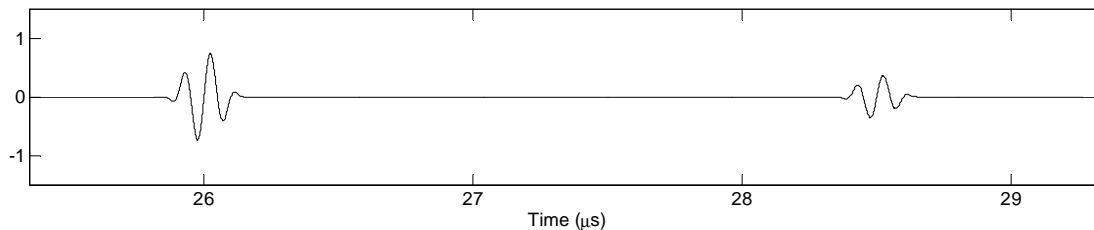


Figure 12: Contribution of ray 1 to the final waveform.

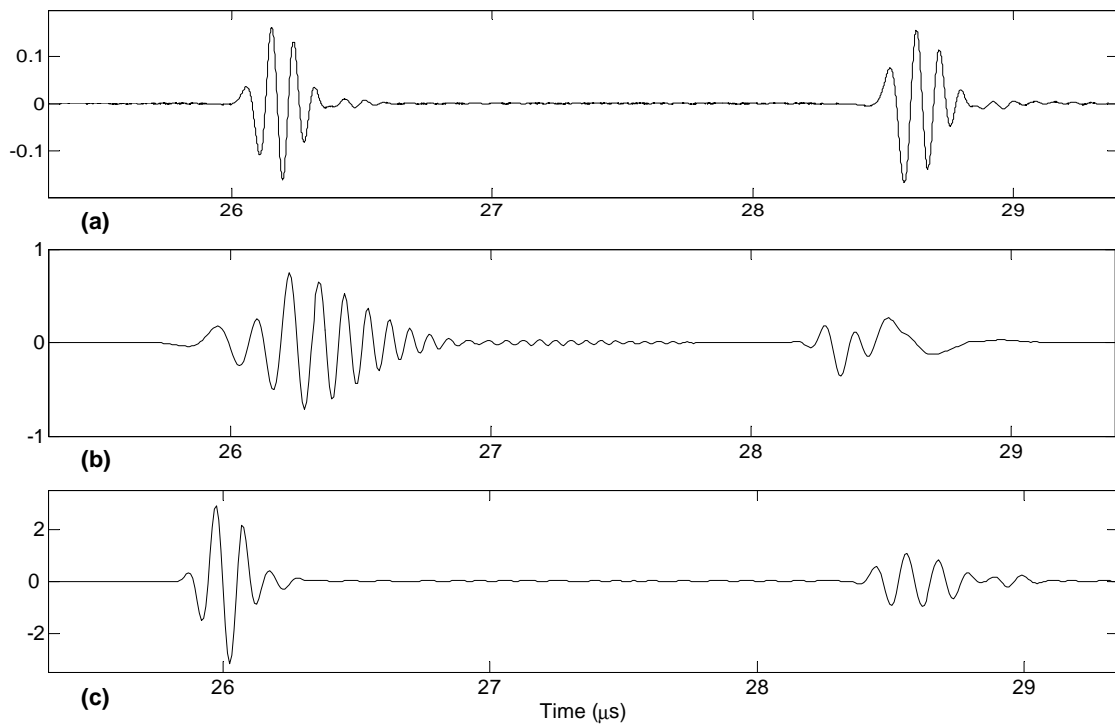


Figure 13: Waveforms obtained for the through-transmission in a cylindrical waveguide of length 152.4 mm (6") and diameter 9.53 mm (3/8"), (a) Experimental. (b) Simulated with finite difference. (c) Simulated with ray tracing.

CHAPTER IV

WAVEGUIDE OPTIMIZATION

This chapter considers the design of waveguides that provide attenuation of trailing echoes while satisfying the constraints associated with the specific application of pipeline monitoring.

4.1 Rod Dimensioning

The first step in the design of the waveguide is the choice of its dimensions. The diameter and length of the rod have a direct impact on the amount of mode conversions, and thus on the energy partition between the echoes. However, the choice of the dimensions cannot be based exclusively on the minimization of trailing echoes. For example, thermal issues also need to be taken into account.

4.1.1 External Constraints

In the context of pipeline inspection, a set of constraints apply on rod dimensions. First, the curvature of pipe walls requires small rod diameters to allow attachment. However, the diameter has to be large enough to achieve a good signal-to-noise ratio. Additionally, the rod should not be too long to avoid signal loss. Finally, waveguides are used to keep transducers away from high temperature areas. As a result, the heat transfer through the waveguide has to be limited. From this perspective, the rod should be as long as possible and its diameter as small as possible.

4.1.2 Influence of Rod Diameter on Signals

The diameter has several impacts on the waveform. First, the smaller the diameter, the more mode conversions there are, and the more energy is transferred from the

first arrival to trailing echoes. The diameter also influences the echo spacing. This is an important effect as insufficient echo spacing can result in echoes overlapping, making thickness measurement impossible.

Three rods of length 101.6 mm (4") and respective diameters of 9.54 mm (3/8"), 12.7 mm (1/2") and 19.05 mm (3/4") were tested in pulse-echo mode to illustrate these effects. Results are presented in Figure 14 and confirm the two effects cited above.

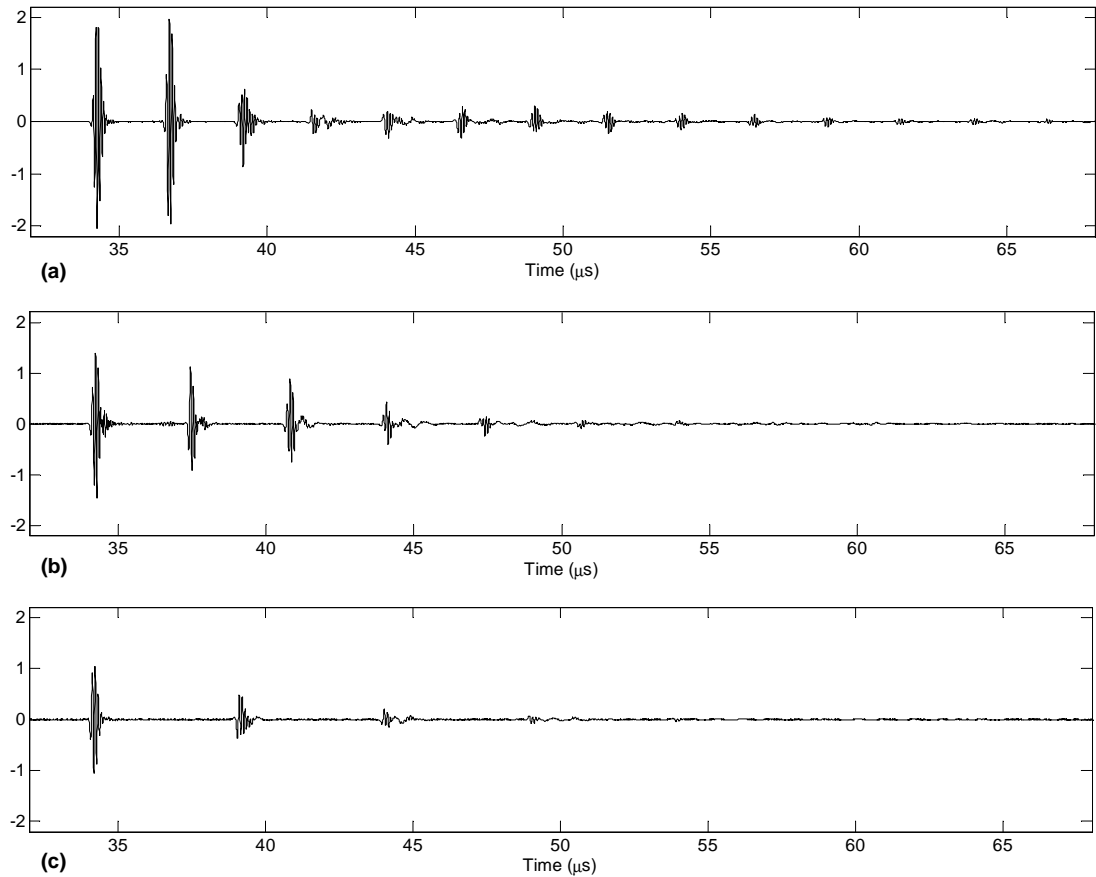


Figure 14: Comparison of pulse-echo waveforms for rods of same length 101.6 mm (4") and different diameters (a) diameter 9.47 mm (3/8"). (b) diameter 12.64 mm (1/2"). (c) diameter 18.98 mm (3/4").

Table 3 compares the experimental and theoretical time delays between the first arrival and the first trailing echo for the three rod diameters considered here; the

agreement is excellent.

Table 3: Comparison of the experimental and theoretical data available for the time delay between the first arrival and the first trailing echo.

Rod Diameter (mm)	Theoretical Δt (μs)	Experimental Δt (μs)
9.47	2.47	2.47
12.64	3.29	3.32
18.98	4.95	4.97

4.1.3 Influence of Rod Length on Signals

The impact of the rod length is also twofold. The longer the rod, the more energy is transferred to trailing echoes since more mode conversions occur. Also, the arrival time of the entire train is delayed when the length of the rod increases. However, every echo is shifted by the same amount and this does not impact thickness measurements.

Experimental waveforms were acquired in pulse-echo mode for three waveguides of diameter 9.54 mm (3/8") and respective lengths of 101.6 mm (4"), 152.4 mm (6"), and 203.2 mm (8"). Results are presented in Figure 15 and confirm the effects listed above.

4.1.4 Discussion and Choice of the Final Dimensions

From a signal point of view, it is better to use a short rod with a big diameter to maximize the spacing between trailing echoes and achieve a large amplitude for the first arrival. However, according to constraints, the diameter should be just large enough to get a good signal-to-noise ratio, and the rod must be long enough for thermal protection of the transducer.

The thickness of pipe walls ranges between 9.54 mm (3/8") and 25.11 mm (1"), which results in times-of-flight through the specimen between 3.1 μs and 6.9 μs . Consequently, there is at least one trailing echo in the range of arrival times of the

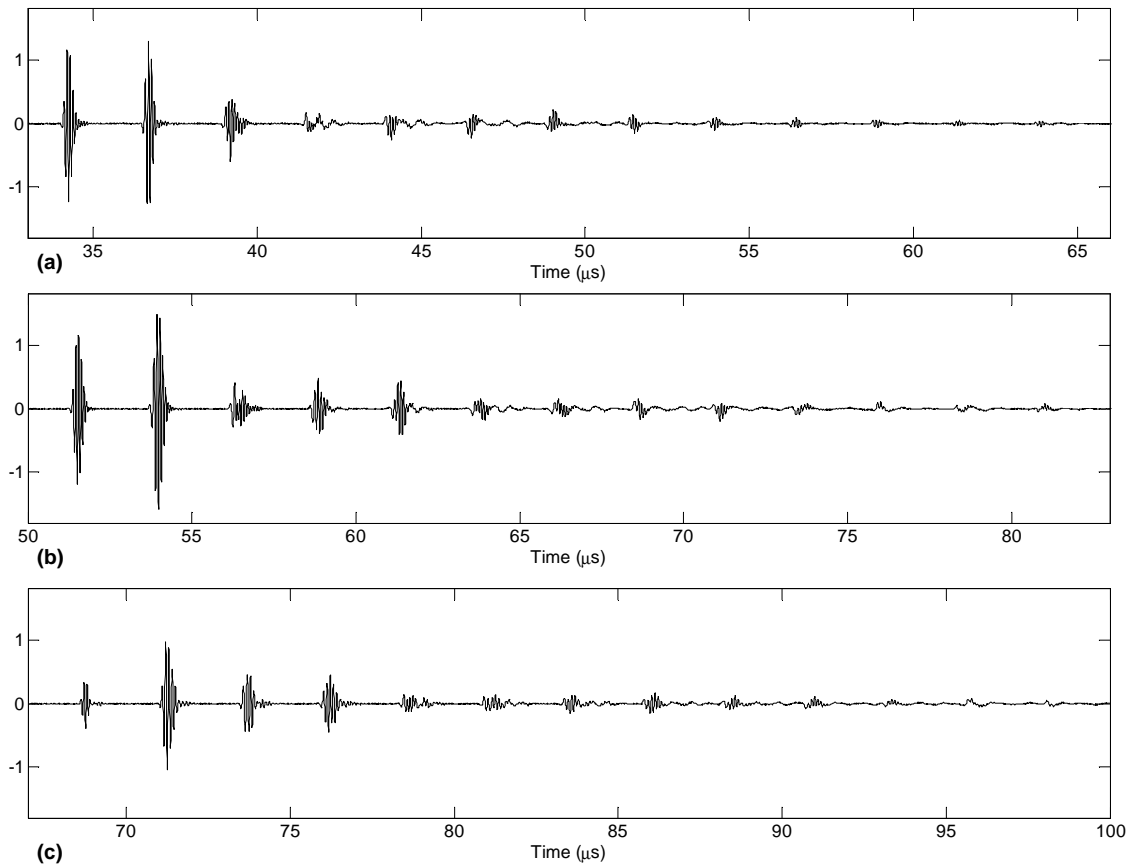


Figure 15: Comparison of pulse-echo waveforms for rods of same diameter ($3/8''$) and different lengths (a) length 101.6 mm ($4''$). (b) length 152.4 mm ($6''$). (c) length 203.2 mm ($8''$).

backwall echo for every tested diameter. Rods without trailing echoes in this range would have a diameter larger than 26.5 mm, which is too large from both attachment and thermal points of view. The intervening trailing echo needs to have a negligible amplitude in comparison with the backwall echo to enable thickness measurements. Figures 14 and 15 showed that in the range allowed by the application, the modification of the dimensions of the rod was not sufficient to attenuate the trailing echoes. Other more effective methods were presented in chapter II for trailing echo attenuation. Consequently, the dimensions of the waveguide are chosen in accordance with the external constraints. Note that the chosen diameter needs to be large enough to give a sufficient signal-to-noise ratio and a sufficient echo spacing. Concerning the length, it needs to be large enough to create a temperature gradient and penetrate the insulation. However, it should not be too long or the signal-to-noise ratio will decrease and the rod will excessively protrude from the pipe. It was thus decided to use a 152.4 mm (6") long rod with a diameter of 9.54 mm (3/8"). The corresponding pulse-echo waveform is that of Figure 15(b). It is anticipated that a means of coating the rod will be required, although that is outside of the scope of this thesis.

4.2 Impact of the Source on Trailing Echoes

Mode conversions are based on Snell's law, and any modifications of the angle of incidence modify them. Usually, transducers are modeled as emitting with a straight beam, which is not an acceptable approximation for the propagation in waveguides. In reality, the transducer has beam spread as illustrated in Figure 16. The corresponding emitted wave is thus subjected to numerous mode conversions on waveguide boundaries, resulting in the generation of trailing echoes.

The beam spread angle for the Olympus transducers used in this study can be estimated in the far field as [26],

$$\alpha = 0.514 \frac{c}{fD}, \quad (11)$$

$$N = \frac{D^2 f}{4c}, \quad (12)$$

where f is the frequency, D is the transducer diameter, c is the wave velocity, and N is the near field distance.

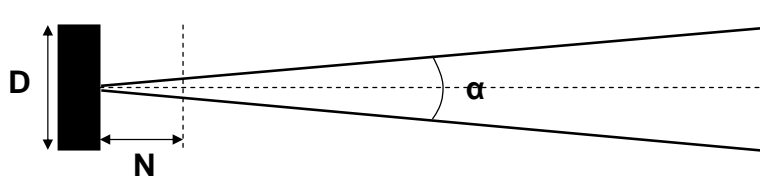


Figure 16: Model of transducer emission.

The velocity of waves depends upon the material, which has to be the same as the pipe walls to enable the welding operation. However, the diameter and the frequency of the transducer can be tuned to change the angle of the beam. Their impacts are similar and thus there is no need to study both. It is thus decided to limit the study to the influence of the transducer diameter on trailing echoes.

The formula being valid in the far field only, the average near field distance needs to be estimated. It is 40 mm for the transducer used here, which is not negligible in the rods considered for experiments. In the near field, waves travel in every direction and many mode conversions can occur, thus contributing to trailing echo generation.

Theoretical studies based on the formula 11 are not sufficient to study the impact of the transducer diameter on trailing echoes. Besides, the limited number of transducers in the diameter range studied does not allow precise experimental studies. As a result, it is decided to study the impact of the transducer diameter on trailing echoes through simulations. Experimental measurements are then made for verification purposes.

Through-transmission waveforms were simulated through ray tracing for cylindrical waveguides of length 152.4 mm (6") and diameter 9.54 mm (3/8"), with transducer diameters ranging between 0.5 mm and 9.5 mm. The distance between two point sources used to model the transducers is set constant and equal to 0.2 mm. Diameter variations were then implemented by adding or removing point sources. To compensate for the variation in transmitted energy from one transducer to the other, waveforms were normalized before comparison. In a through-transmission configuration with the waveguide dimensions chosen here, most of the energy is split between the first arrival and the first trailing echo. Thus, the attenuation of trailing echoes can reasonably be quantified through the amplitude ratio between the first trailing echo and the first arrival. The other trailing echoes experimentally proved to be smaller than the first one for every transducer diameter.

The results of simulations are presented in Figures 17 and 18. It appears that there exists an optimal transmitter diameter such that the cleanest waveform is obtained for through transmission in the waveguide considered. However, the improvement brought by the choice of the optimal diameter is not that significant and definitely not sufficient to significantly improve measurements with waveguides. Experiments were made with three transducers of diameters 3.175 mm (0.125"), 6.4 mm (0.25"), and 9.5 mm (0.375"), but the variation of the attenuation was too small to be detected. It is thus concluded that the influence of the transducer diameter on trailing echoes is negligible.

4.3 Influence of Boundary Modifications on Trailing Echoes

The background section discusses several solutions for the attenuation of trailing echoes based on waveguide design. Although giving the best results, clad rods are not considered here because they are judged to be incompatible with the welding operation. In addition, their manufacturing is expensive, which reduces their appeal

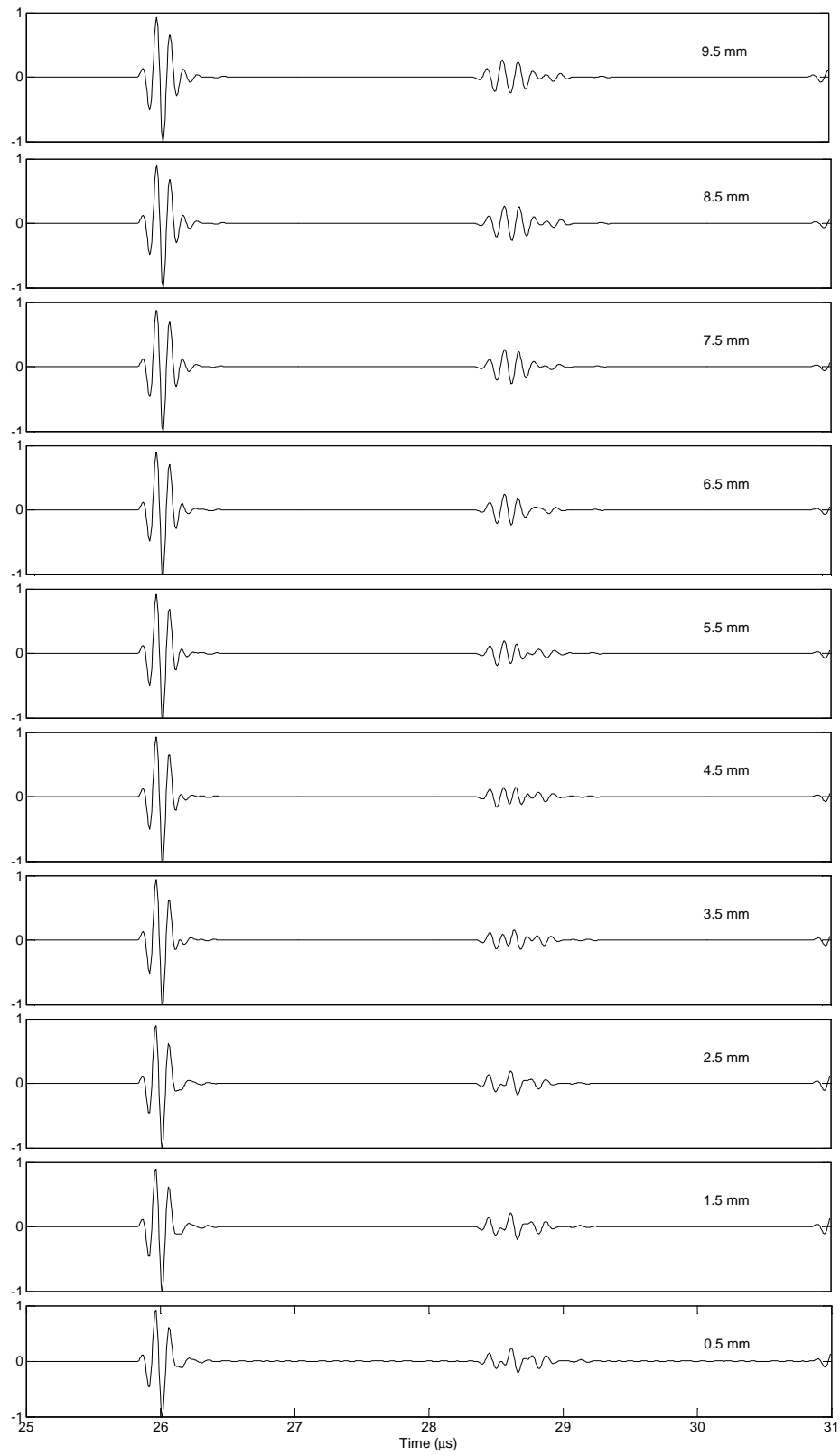


Figure 17: Through-transmission waveforms in a cylindrical rod of length 152.4 mm (6") and diameter 9.54 mm (3/8") for several transducer diameters.

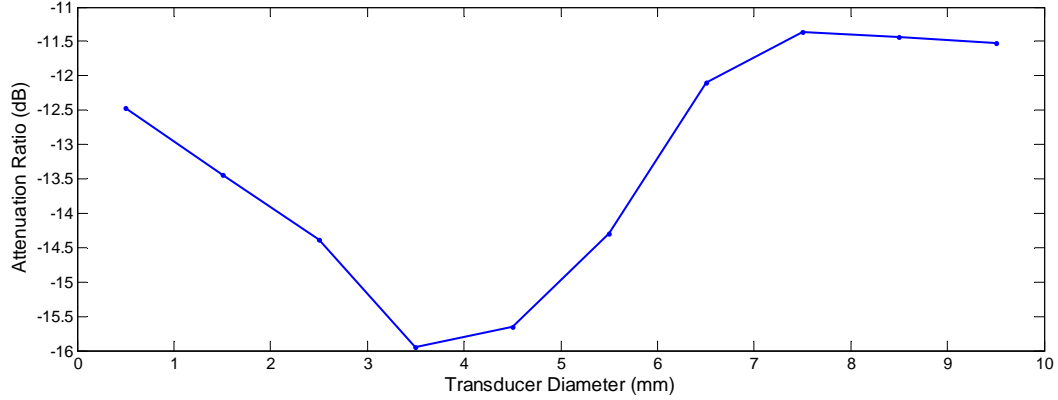


Figure 18: Relative attenuation of the trailing echoes with transducer’s diameter.

for large scale implementation. For the specific needs of the application considered here, tapered rods provide a reasonable compromise. They can be machined from any material, are inexpensive, and give reasonably good results for the attenuation of trailing echoes.

According to the literature, cleaner signals are obtained when the taper angle increases [15]. However, the link between the taper angle and the attenuation of the trailing echoes has not been explicitly shown. In order to get the best design available, it was thus decided to study the influence of the taper angle on trailing echoes.

Preliminary measurements were performed by acquiring the signals resulting from pulse-echo and through-transmission measurements for a 0.75 degree taper angle. Figure 19 presents the corresponding results. As expected by reciprocity [27], the two through-transmission signals are almost identical. In contrast, the two pulse-echo signals are totally different. The waveform obtained with the source at the small end is relatively clean, although lower in amplitude, while the signal obtained with the source at the large end shows improvements on the first trailing echo only. The other trailing echoes are amplified. According to table 3, two trailing echoes fall in the range of arrival times of the backwall echo for the rod of diameter 9.54 mm (3/8”) chosen. Additionally, the trailing echoes tend to have earlier arrival times when the

taper angle increases. Thickness measurements are not possible in this configuration and they are not considered.

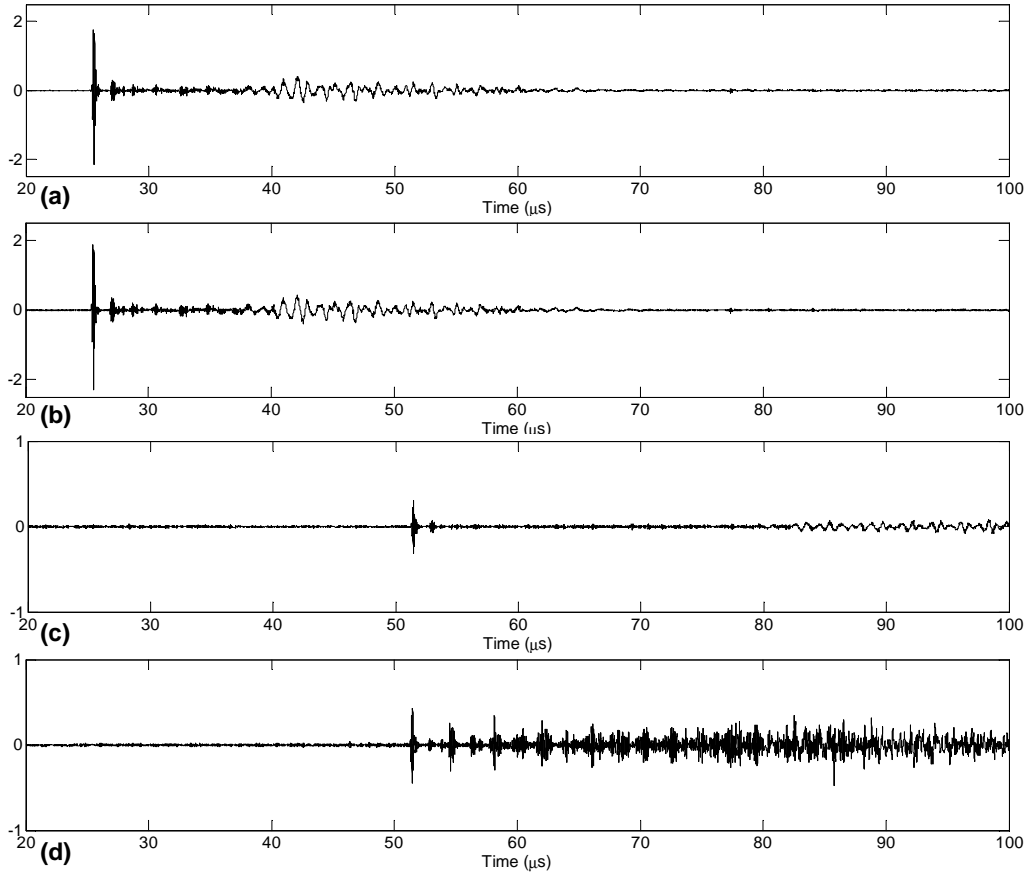


Figure 19: Waveforms recorded in different measurement configurations on a 0.75° tapered rod of length 152.4 mm (6”) and larger diameter 9.54 mm ($3/8$ ”). (a) Through-transmission configuration with source at the small end. (b) Through-transmission configuration with source at the large end. (c) Pulse-echo configuration with source at the small end. (d) Pulse-echo configuration with source at the large end.

Finally, the trends are the same for pulse-echo measurements from the small end and for through-transmission. As a result, the study is carried out in through-transmission mode for simplification of the simulations.

4.3.1 Experimental Observations

In order to capture the major trends linked with the introduction of a taper angle, through-transmission signals were acquired for five rods of respective taper angles

of 0° , 0.25° , 0.5° , 0.75° , and 1° . The transmitter was clamped to the large end of constant diameter 9.53 mm ($3/8''$), while the receiver was hand-coupled to the small end. For more reliability, a total of six waveforms were acquired for each taper angle. Only the first two echoes were considered since the other trailing echoes experimentally proved to be smaller than the first one for the range of taper angles considered. Sample waveforms are presented for each rod in Figure 20. Note that the amplitude of the first arrival decreases as the taper angle increases. This effect could be deleterious if the noise level was too high, but as long as the signal-to-noise ratio is sufficient, it does not constitute a problem.

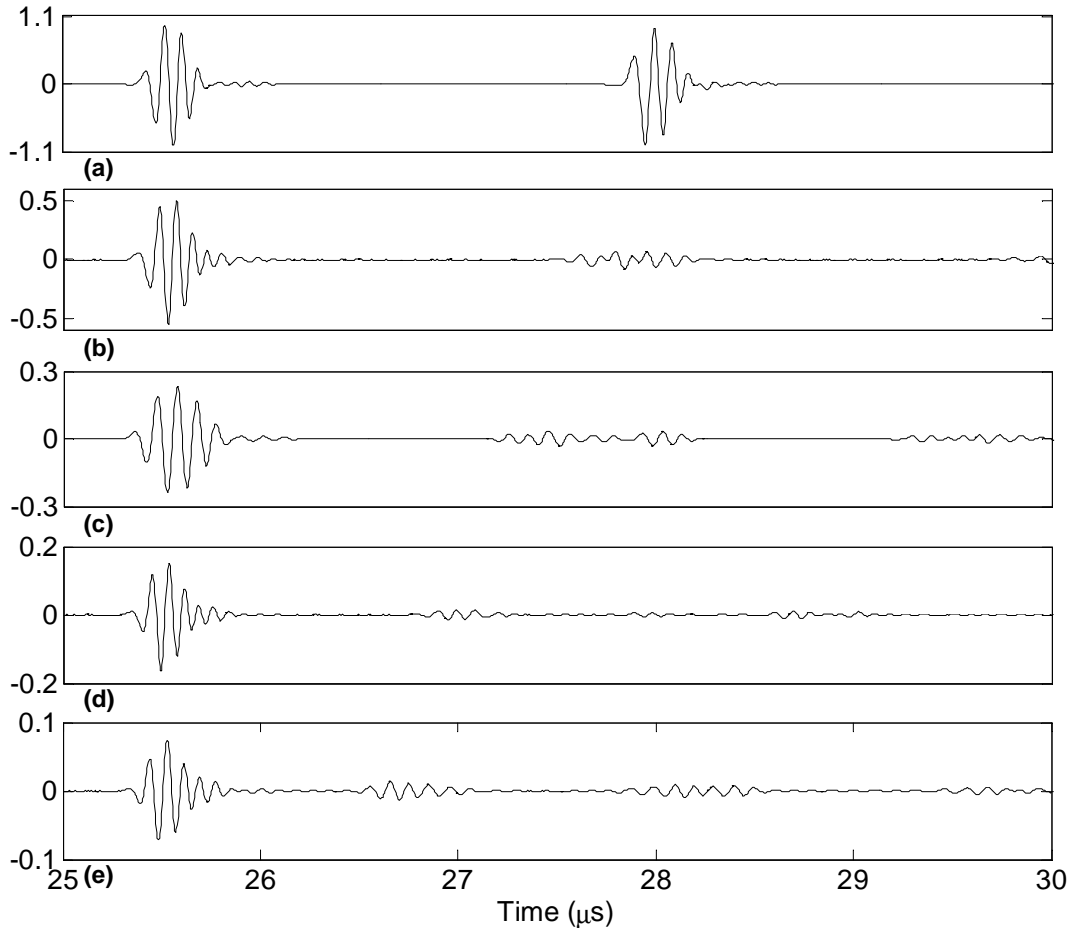


Figure 20: Experimental waveforms for different taper angles on a waveguide of length 152.4 mm ($6''$) and diameter 9.54mm (a) straight rod. (b) 0.25° taper angle. (c) 0.50° taper angle. (d) 0.75° taper angle. (e) 1° taper angle.

As expected, the relative amplitude of the first trailing echo decreases when a

taper angle is introduced. Once again, the attenuation was quantified through the amplitude ratio between the first trailing echo and the first arrival. The resulting data are presented in Figure 21.

The limited data shown here indicates that for larger taper angles, the increase of the taper angle does not necessarily reduce the relative amplitude of the trailing echoes. A close look at the waveforms shows that the trailing echoes tend to split and spread out in time as the taper angle increases, which contributes to noise or clutter behind the first arrival. As a result, after a certain amount of taper, any increase in the taper angle results in a deterioration of the waveform as the predominant effect becomes echo spreading without a reduction in amplitude. For the specific rods considered here, the optimal angle marking the limit between signal improvement and signal deterioration is between 0.25° and 0.75° .

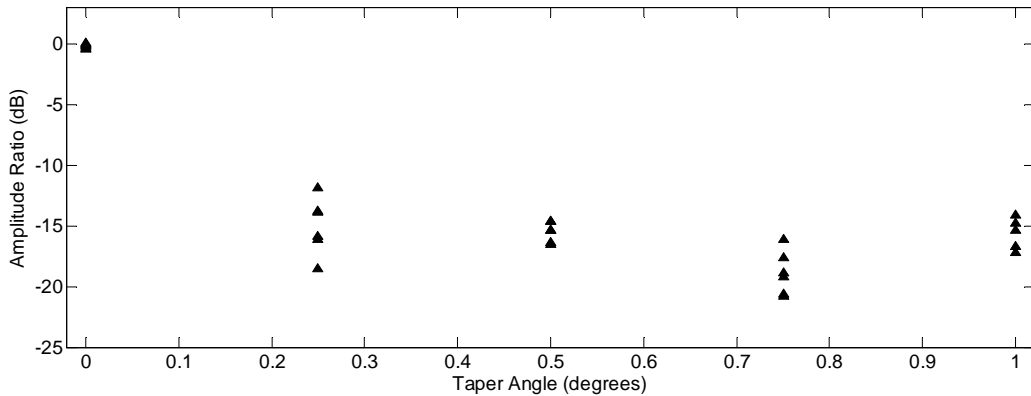


Figure 21: Amplitude of the first trailing echo relative to the first arrival versus taper angle. Each data point represents a separate waveform acquisition.

Experimental results are not precise enough for a fine study of the impact of the taper angle. In addition, the cost of machining rods can be avoided by going to simulations. The 2D models introduced in chapter 3 are thus used to obtain a better understanding of the taper angle influence on trailing echoes and attempt to determine the bounds for the optimal angle. Note that models always have imperfections, especially here where a 2D model is used to represent a 3D environment. Results

thus need to be analyzed keeping in mind the approximate nature of the simulations.

4.3.2 Results of Simulations

Simulations were performed for 21 taper angles from 0° to 1° with an increment of 0.05° . The attenuation of trailing echoes was quantified by the amplitude ratio between the first trailing echo and the first arrival. Results obtained for finite differences are presented in Figures 22 and 23.

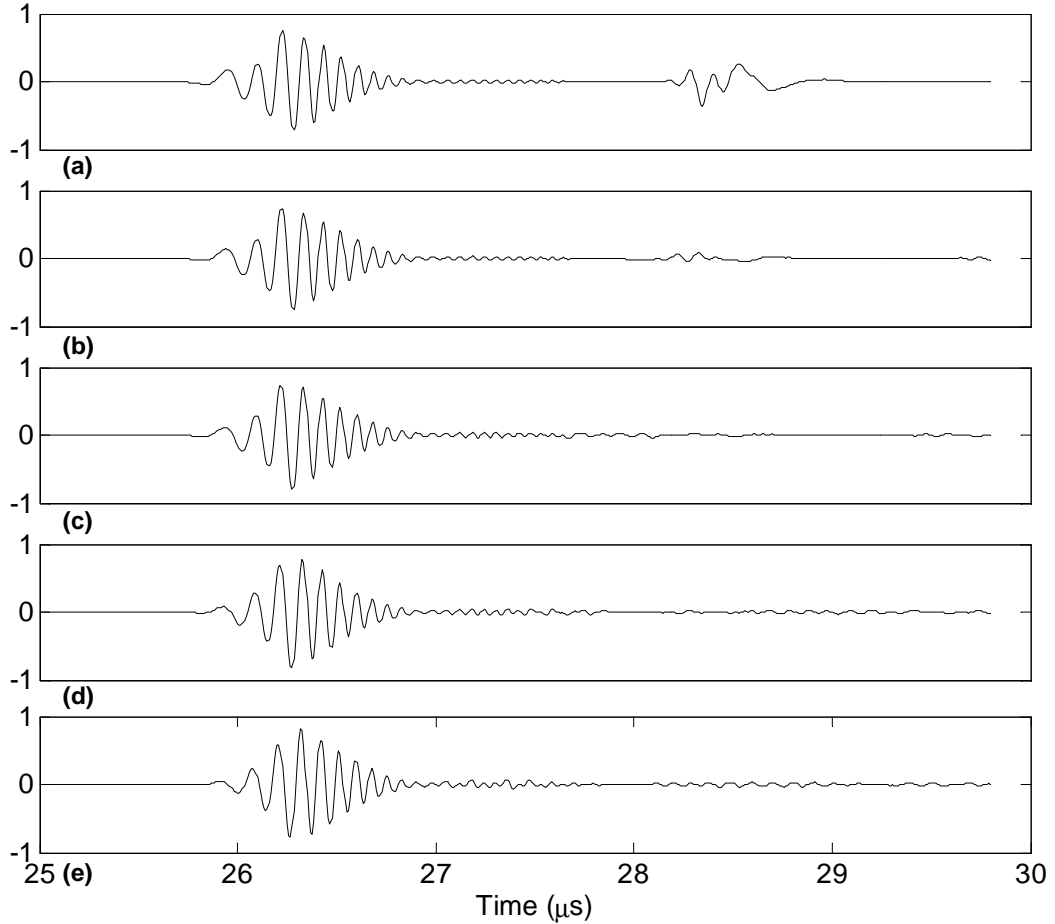


Figure 22: Waveforms resulting from finite difference simulations for different taper angles on a waveguide of length 152.4 mm (6”) and diameter 9.54 mm (3/8”) (a) straight rod. (b) 0.25° taper angle. (c) 0.50° taper angle. (d) 0.75° taper angle. (e) 1° taper angle.

Though attenuation of trailing echoes is observed when the taper angle increases, this model has several imperfections. First, it does not reflect the amplitude decrease of the first arrival when the taper angle increases. At the same time, it underestimates

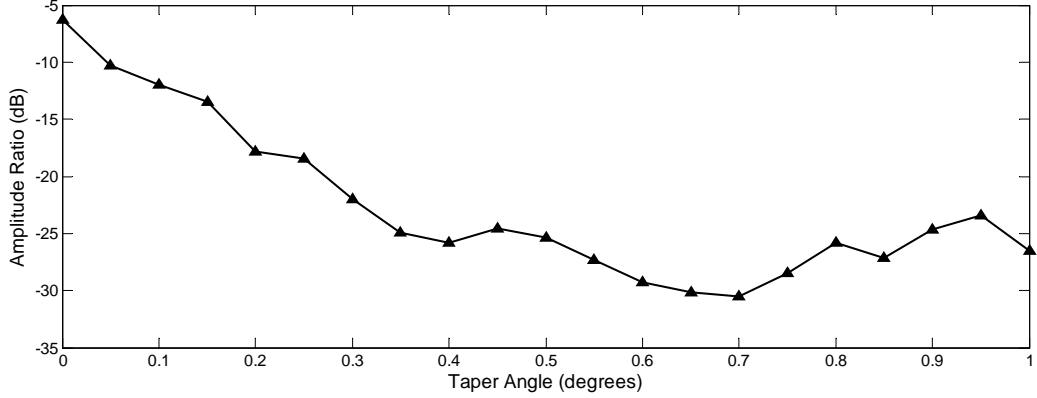


Figure 23: Impact of the taper angle on the trailing echo attenuation with the finite difference model.

the amplitude of trailing echoes. Finally, the finite difference grid creates simulation noise that precludes trailing echo analysis for taper angles larger than about 0.4 degree. Any determination of an optimal angle is thus impossible with this model. However, the results obtained with finite differences can be compared to the results of ray tracing to determine if imperfections come from the lack of 3D considerations.

Ray tracing results are presented in Figures 24, 25 and 26. Figure 25 shows the same signals as Figure 24 but with different vertical scales for each signal to better see the trailing echoes. As expected, this model allows the exploration of angles larger than 0.4 degrees since there is no simulation noise. In addition, it captures the echoes shifting and spreading that could not be observed with finite differences. However, the respective amplitudes of each echo are still not in agreement with experiments.

To better understand the imperfection of models and thus learn about wave propagation in tapered rods, all data are presented in Figure 27. Interestingly, the results obtained for ray tracing and finite difference are in reasonably close agreement for taper angles smaller than 0.4 degree. After this amount of taper, results are not comparable anymore due to the simulation noise introduced in the finite difference model. This observation indicates that the misrepresentation of amplitudes in simulated waveforms is likely linked with the lack of 3D considerations.

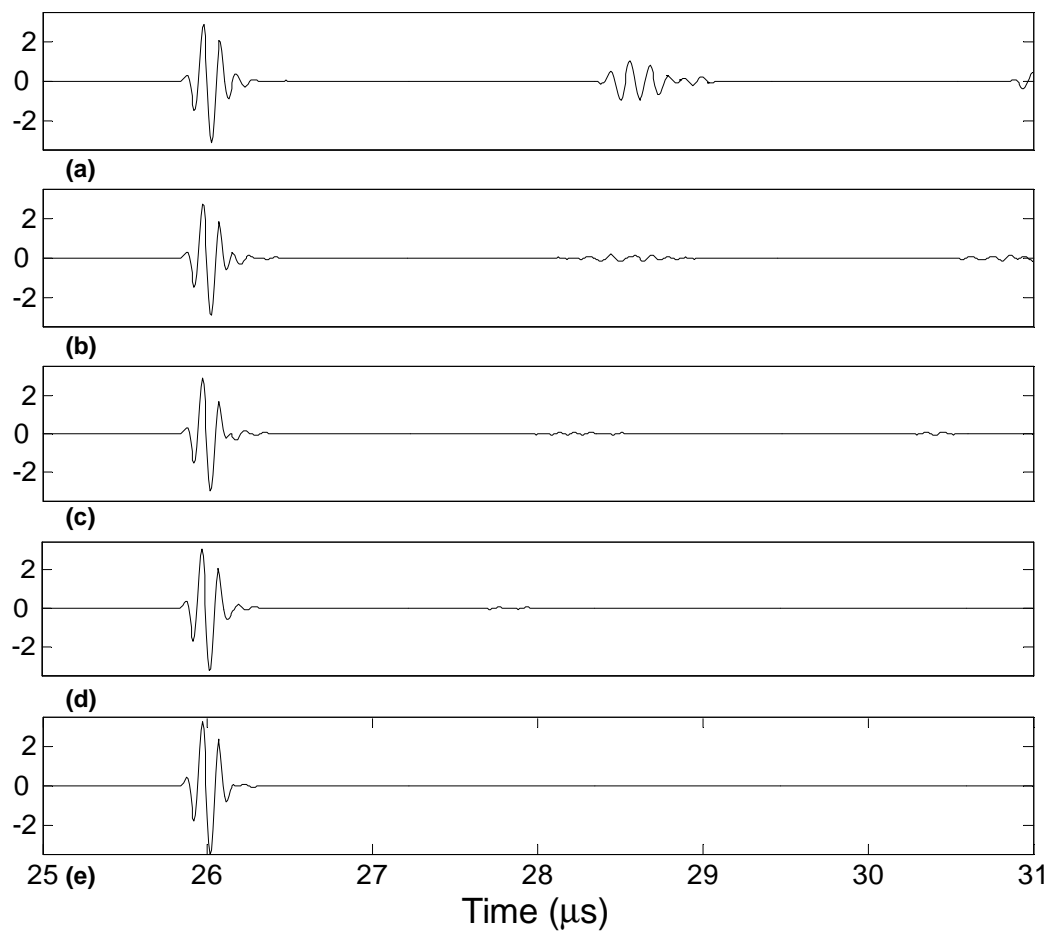


Figure 24: Waveforms resulting from ray tracing simulations for different taper angles on a waveguide of length 152.4 mm (6") and diameter 9.54mm (3/8") (a) straight rod. (b) 0.25° taper angle. (c) 0.50° taper angle. (d) 0.75° taper angle. (e) 1° taper angle.

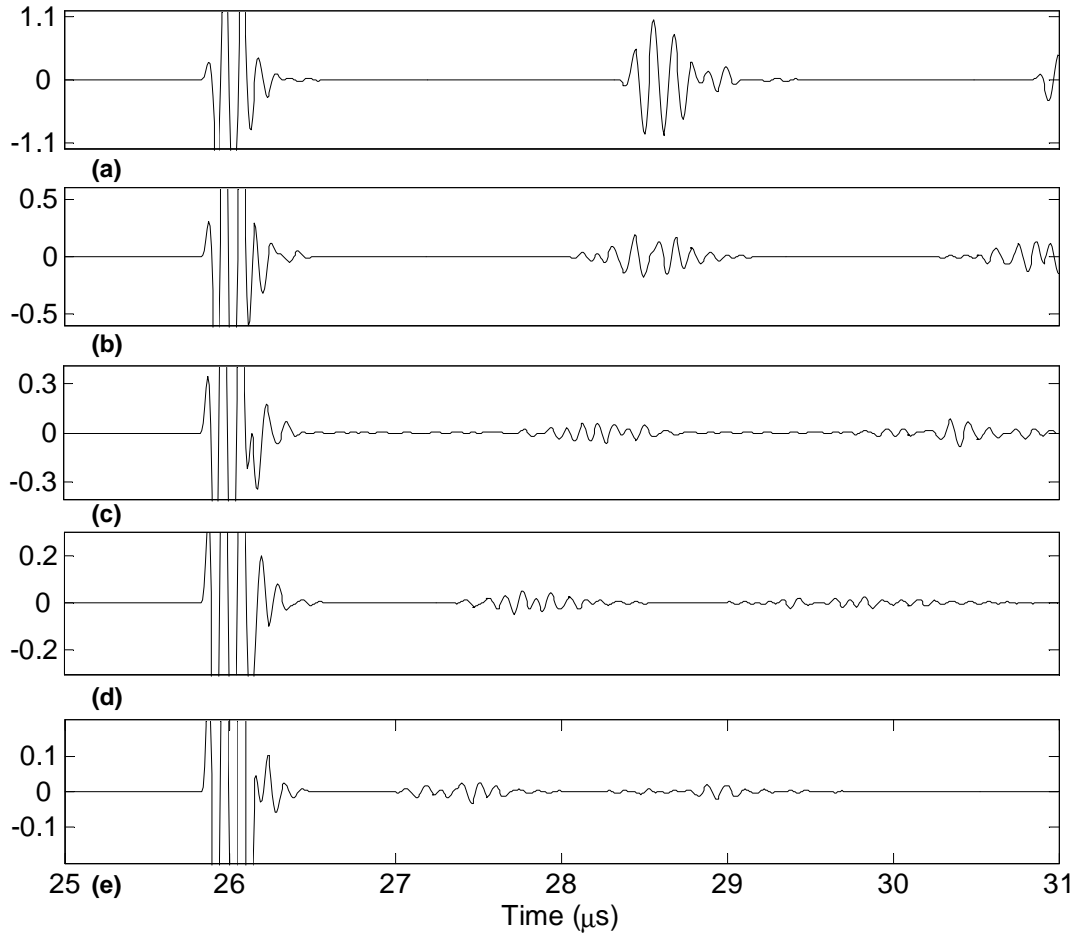


Figure 25: Same as Figure 24 after zooming on the trailing echoes (a) straight rod. (b) 0.25° taper angle. (c) 0.50° taper angle. (d) 0.75° taper angle. (e) 1° taper angle.

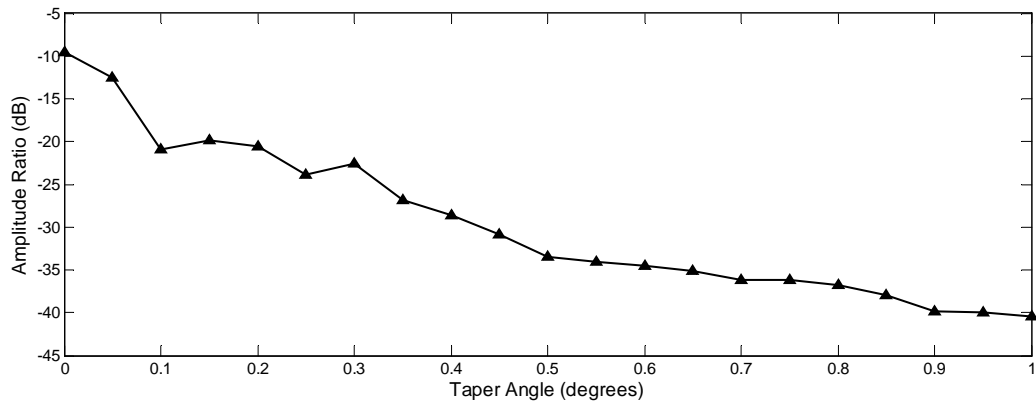


Figure 26: Impact of the taper angle on the trailing echo attenuation with the ray tracing model.

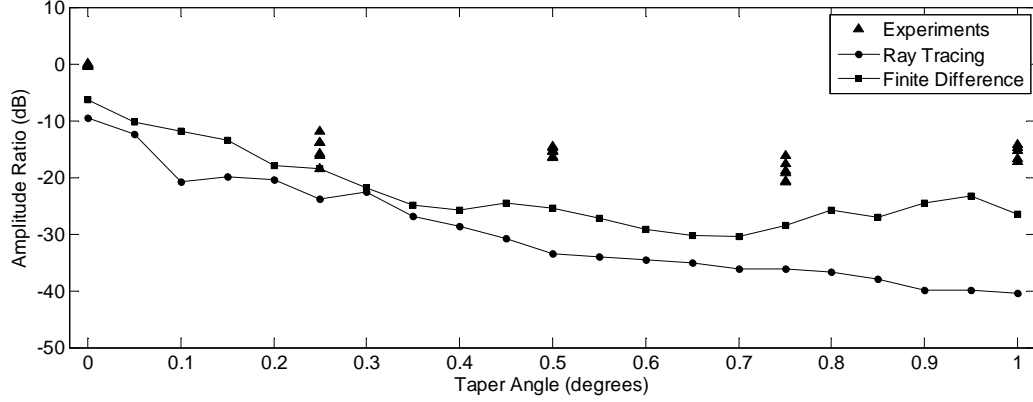


Figure 27: Comparison of trailing echo amplitude ratios from experiments and both simulations.

The representation of rods by their cross-sections limits the study to radial contributions. However, in reality rays are emitted in every direction and off-axis rays should be represented. These rays undergo more reflections as they “spiral” down the rod and they are subjected to curvature effects. As a result, their amplitudes are primarily transferred to trailing echoes. The consideration of these rays in the ray tracing model would be expected to give a more realistic amplitude partition between the first arrival and the trailing echoes.

To conclude, better results could be obtained with 3D models, but at the expense of a large increase in the computational time. The 2D models presented here, particularly the ray tracing model, already allow a good understanding of the wave propagation in tapered rods and are sufficient to understand the impact of the taper angle on trailing echoes.

4.3.3 Qualitative Analysis of the Results

Though precise quantification of results is not possible with the data reported here, the simulations gave a better understanding of the taper angle impact on trailing echoes. Specifically, the modeling of waves through propagating rays greatly helps in studying the evolution of waveforms. In this context, each echo is the result of the

constructive interference of multiple ray contributions. The study of how the echoes evolve can then be understood by studying their components. The n^{th} trailing echo is subsequently referred as the trailing echo of “order n ” to simplify the explanation.

In a straight rod, trailing echoes are composed of ray contributions with similar arrival times that constructively interfere. When a taper angle is introduced, the rod diameter is not constant and its variations result in a wider range of arrival times for each contribution, which reduces the constructive interference effect and thus reduces the amplitude of the trailing echoes. Figure 28 illustrates the influence of the diameter variations on the arrival times. The first arrival is less impacted by diameter variations since most of its contributions are provided by rays that never hit boundaries.

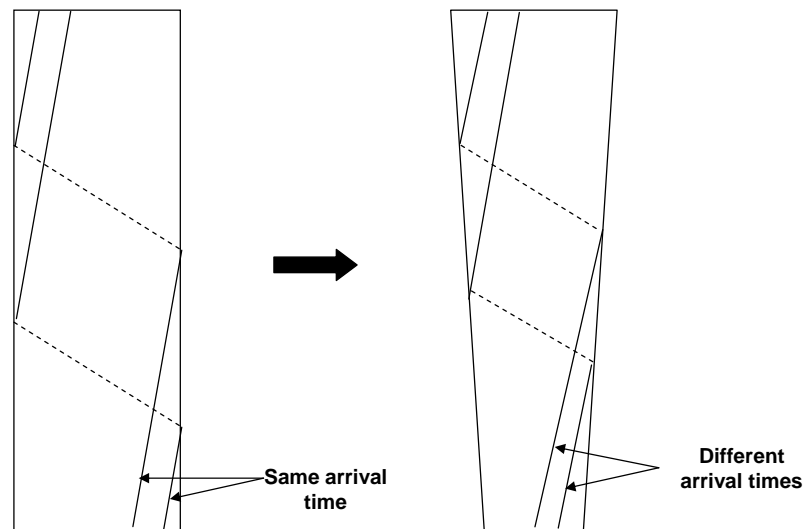


Figure 28: Change in arrival times of trailing echo rays after introduction of a taper angle.

Another effect of the taper angle is a variation in the number of mode conversions.

When traveling from the large end to the small end of the rod, the number of mode conversions increases with respect to the straight rod case, while it decreases when traveling in the opposite direction. Consequently, the amplitude of each contribution as well as the energy partition between the echoes is modified. In addition, the incidence angle on boundaries is modified by the taper angle, which also has an impact on the energy partition.

The taper angle also interacts with the transducer beam angle. When traveling from the small end to the large end, the beam tends to focus, while it spreads in the opposite direction. As a result, when the transducer is at the larger end, waves are subjected to more mode conversions on their round-trip than in the case when the transducer is at the smaller end, and how the energy is partitioned is also affected.

To summarize, the introduction of a taper angle results in two primary effects. First, the arrival times of the ray contributions to a single trailing echo split and spread out, which reduces the amplitude of that echo. Second, the energy partition is modified. Energy tends to be transferred to higher order trailing echoes when waves propagate from the large end to the small end, while the opposite effect occurs in the opposite direction. At the same time, more energy is transferred towards the trailing echoes if the transducer is at the large end.

Signal improvements mainly result from the widening of the range of arrival times for the ray contributions of each trailing echo. This effect is not as strong on every trailing echo. The higher the trailing echo order, the smaller the impact of the taper angle. In long rods, the impact is always important even on high order trailing echoes, but in shorter rods, the “widening effect” only applies to low order trailing echoes. This behaviour can be explained with geometrical considerations. Figure 29 presents the paths of contributions to the two first trailing echoes in a short tapered rod. When considering the ray contributions to the first trailing echo, there is a significant number of paths that are very different, and the introduction of the taper angle has

a real impact on the echo amplitude. Concerning the contributions to the second trailing echo, the number of possible paths is reduced and the diameter variations have similar impacts on multiple contributions. As a result, several contributions still have very similar arrival times and they continue to interfere constructively.

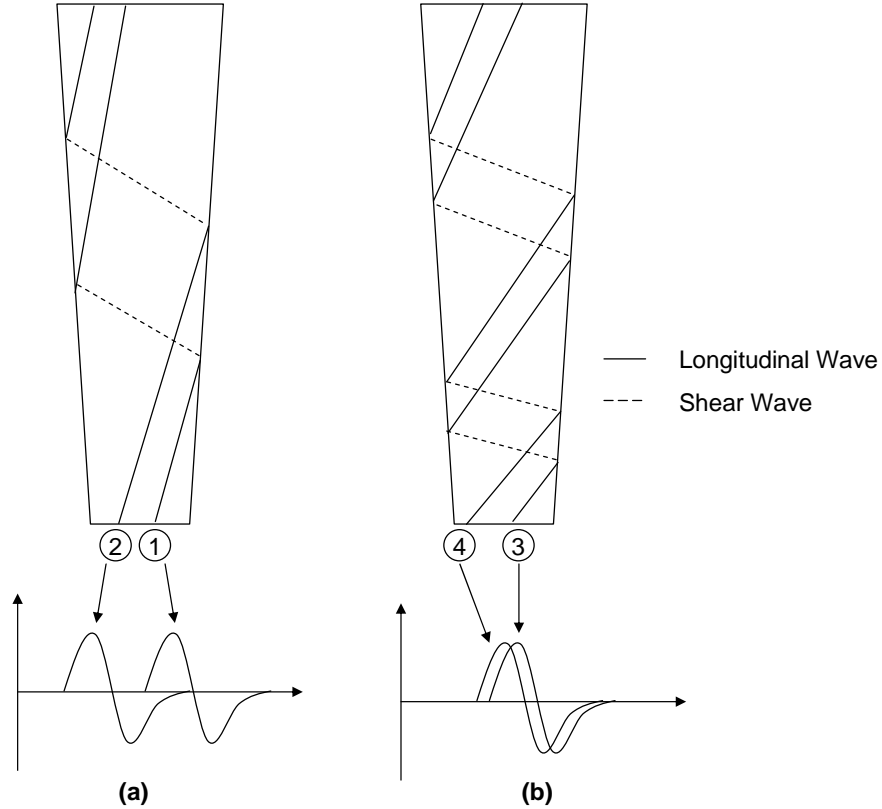


Figure 29: Variability of the "widening" effect with the trailing echo order. (a) First order trailing echo order. (b) Second order trailing echo.

With these considerations, it becomes possible to explain the lack of improvement on the pulse-echo signal of Figure 19(d). The transducer was coupled to the large end of a short tapered rod of angle 0.75° . The amount of mode conversions was thus important and the energy was essentially transferred to high order trailing echoes on which the "widening effect" was negligible. It can be seen that the first trailing echo is attenuated while the higher order trailing echoes have a large amplitude. The signal

of Figure 19(c) is nicer, because the transducer is at the small end and the reverse effect occurs. The beam angle decreases, reducing the number of mode conversions, and keeping energy in low order trailing echoes on which the "widening effect" is effective. The difference between the total energy of signals (c) and (d) is due to the difference in the area of the rod in contact with the transducer.

The case of long rods was studied in the literature, and results showed that every trailing echo was attenuated when the taper angle increased, which confirms the efficiency of the "widening effect" on every trailing echo.

4.3.4 Summary

For the specific rods considered here, pulse-echo measurements from the large end of tapered rods are not effective. For the other measurement configurations, signal improvements can be obtained by the introduction of a taper angle. An optimal angle can be determined as giving the best signals for the rod dimensions chosen. However, improvements are limited due to the short length of the rods.

The determination of this optimal angle requires 3D modeling, which significantly increases the computational time and will be implemented later only if needed. Further improvement can be obtained with longer rods as presented in the literature. However, an increase in the length may require a diameter increase as well to allow sufficient tapering. In addition, the set of external constraints needs to be respected.

4.4 *Imperfect Machining*

The previous section showed that tapered rods could bring significant improvements to the signal when correctly dimensioned. However, if rods are not machined perfectly, improvements are limited. Figure 30 illustrates the case where the taper does not cover the full length of the rod. The resulting through-transmission waveform is shown in Figure 31. The presence of a small straight part reinforces the constructive interference of ray contributions, while the taper part keeps spreading the trailing

echoes.

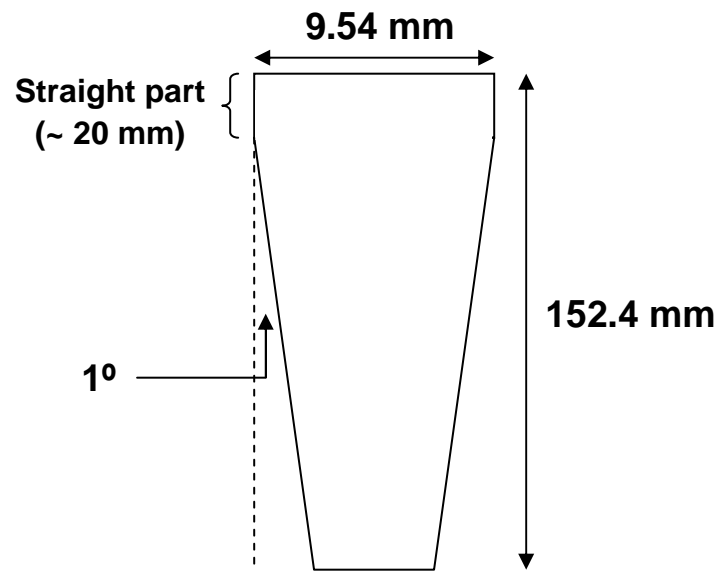


Figure 30: Example of imperfect machining.

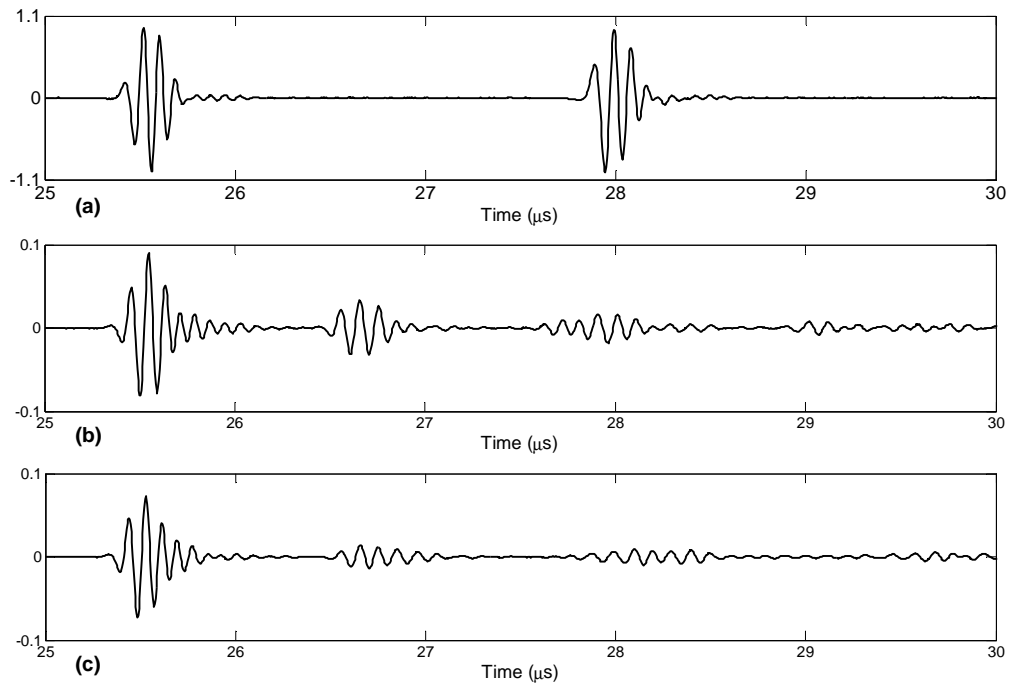


Figure 31: Comparison of two tapered rods with different quality of machining. (a) Bad machining. (b) Good machining.

CHAPTER V

WAVEGUIDE IMPLEMENTATION FOR THICKNESS MONITORING

Different waveguide designs have been studied to attenuate trailing echoes, but their actual implementation still needs to be considered. According to Chapter II, thickness measurements can be performed either in pulse-echo or in pitch-catch configurations. These two methods can be adapted to enable measurements with waveguides and are presented here to support the final design choice.

5.1 Waveguides and Calibration

5.1.1 Calibration Need

Every experimental measurement is inherently prone to errors, and in some cases calibration is essential to enable measurements of the required accuracy. Errors introduced by imperfections in the experimental setup do not evolve over time and can be compensated through initial calibration. However, dynamic errors depend on experimental parameters that can change between two measurements and their compensation is not as easy.

In the context of ultrasonic thickness measurements, the only measured data is the time-of-flight through the specimen t . After initial calibration, the thickness is determined by,

$$h = \frac{c}{2}(t - t_0), \quad (13)$$

where h is the thickness of the specimen, c is the velocity of the longitudinal waves,

and t_0 is the time delay. The parameters c and t_0 are determined through initial calibration.

When the temperature changes, the wave velocity changes and thickness errors result. To evaluate the need for compensation, this error needs to be quantified. The original value of the wave speed used for calculation is c_0 , which was determined via calibration. The calculated thickness is then given by,

$$h_c = \frac{c_0}{2}(t - t_0). \quad (14)$$

The time t is actually that of Eq.(13) and the error in measured thickness is,

$$\Delta h = h_c - h = h\left(\frac{c_0}{c} - 1\right), \quad (15)$$

where h is the actual thickness of the specimen, c_0 is the original wave speed determined during calibration, and c is the actual wave speed.

When using a waveguide, the backwall echo is delayed and its arrival time does not correspond to the time-of-flight through the specimen. Note that the pitch-catch and pulse-echo methods have different paths through the specimen as illustrated in Figure 32. However, the initial calibration removes the effect of this difference and errors resulting from velocity changes are exactly the same for both methods. As a result, no distinction is made between the two methods hereafter.

The arrival time of the backwall echo is given by

$$t = 2.\left(\frac{h + l}{c}\right) + t_0, \quad (16)$$

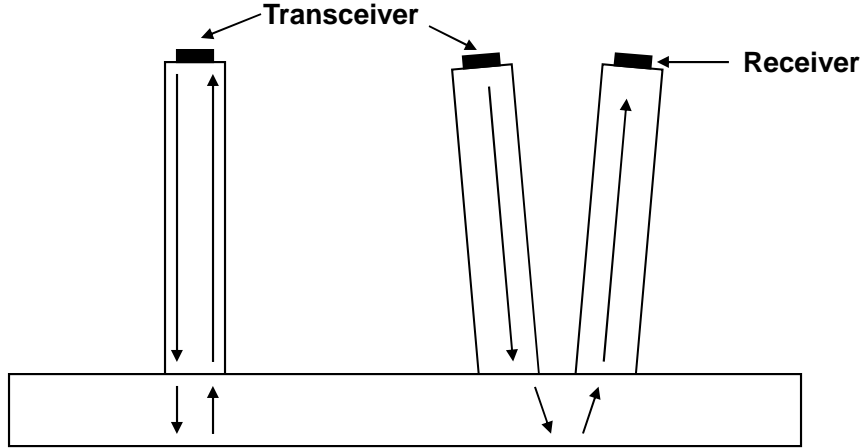


Figure 32: Comparison of the wave paths corresponding to the backwall echo for the pulse-echo and pitch-catch configurations.

where h is the actual thickness of the specimen, l is the actual length of the waveguides, c is the actual wave speed, and t_0 is the initial calibration factor. The initial (calibration) value of the wave speed is c_0 , and the thickness of the specimen is calculated to be,

$$h_c = \frac{c_0 t}{2} - l = \frac{c_0}{c}(h + l) - l. \quad (17)$$

The error of the thickness measurement is given by,

$$\Delta h = h_c - h = (h + l)\left(\frac{c_0}{c} - 1\right), \quad (18)$$

To assess the need for compensation, specific numerical values are considered. The thickness of pipe walls generally ranges between 9.54 mm (3/8") and 25.4 mm (1"), and they are made of steel. The nominal longitudinal wave speed is 5.8 mm/ μ s at room temperature. In accordance with chapter IV, the length of the waveguides is chosen to be 152.4 mm (6"). The resulting errors on thickness measurements are calculated for different temperature variations and are presented in Table 4, using the published values for the longitudinal velocity change with temperature of 0.0006m/s/ $^{\circ}$ C [28].

Table 4: Error introduced by temperature changes in the measured thickness of a 12.7 mm (1/2") plate

Method	ΔT (°C)	Thickness error (%)
contact transducer	10	0.11
contact transducer	100	1.08
contact transducer	500	5.63
waveguide	10	1.43
waveguide	100	14.04
waveguide	500	73.19

For the purpose of monitoring thickness changes caused by corrosion and erosion, an error of 1% is acceptable. Thus, there is no need for calibration with contact transducers for temperature changes up to 100 °C. However, the introduction of a waveguide can result in a significant increase in the measurement error and on-line compensation is necessary.

5.1.2 Dynamic Compensation

When using waveguides, the echo reflected at the interface with the specimen is usually present. The arrival time of this echo corresponds to the time necessary for a round-trip through the waveguide. It can thus be subtracted from the arrival time of the backwall echo to obtain the time-of-flight through the specimen. The dynamic error is then reduced to the error obtained with a contact transducer and it can be neglected.

In the context of high-temperature measurements, it was decided to use welded waveguides to avoid coupling problems. As a result, the interface echo previously used for calibration may disappear or be degraded, and a new solution is needed to enable measurements. In this perspective, it was decided to machine a notch at the welded end of the waveguide. This splits the incoming waves into a reflected and a transmitted wave, and the echo reflected from the notch can be used in the same

Table 5: Impact of the temperature on the measured thickness of a 12.7 mm (1/2") plate after online calibration with the notch echo.

ΔT (°C)	Thickness error (%)
10	0.13
100	1.25
500	6.52

manner as the interface echo to compensate for velocity changes in the waveguide.

Figure 33 presents this concept.

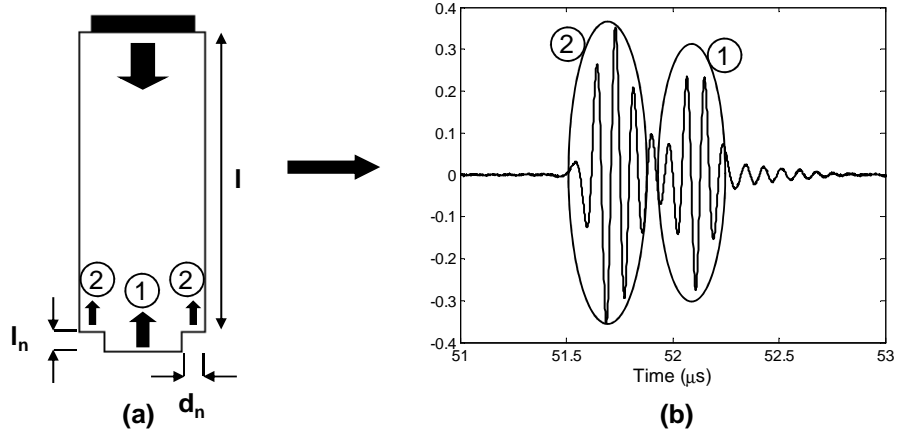


Figure 33: Replacement of the calibration echo through notch digging. (a) Waveguide with a notch. (b) Impact of the notch on the pulse-echo waveform.

The error in measurements is then given by,

$$\Delta h = (h + l_n) \left(\frac{c_0}{c} - 1 \right), \quad (19)$$

where h is the actual thickness of the specimen, l_n is the length of the notch, c_0 is the original wave speed, and c is the actual wave speed.

Table 5 gives values for the measurement error on a plate of thickness 12.7 mm (1/2") for a notch of length 2 mm. Temperature variations are expected to be much less than 100 °C and the error is thus negligible.

The depth of the notch, d_n can then be determined to control the partition between transmitted and reflected waves. Experiments with few notches showed that only a small reflective area is necessary for the notch echo to be detected. The waveforms corresponding to the tested notches are presented on Figure 34.

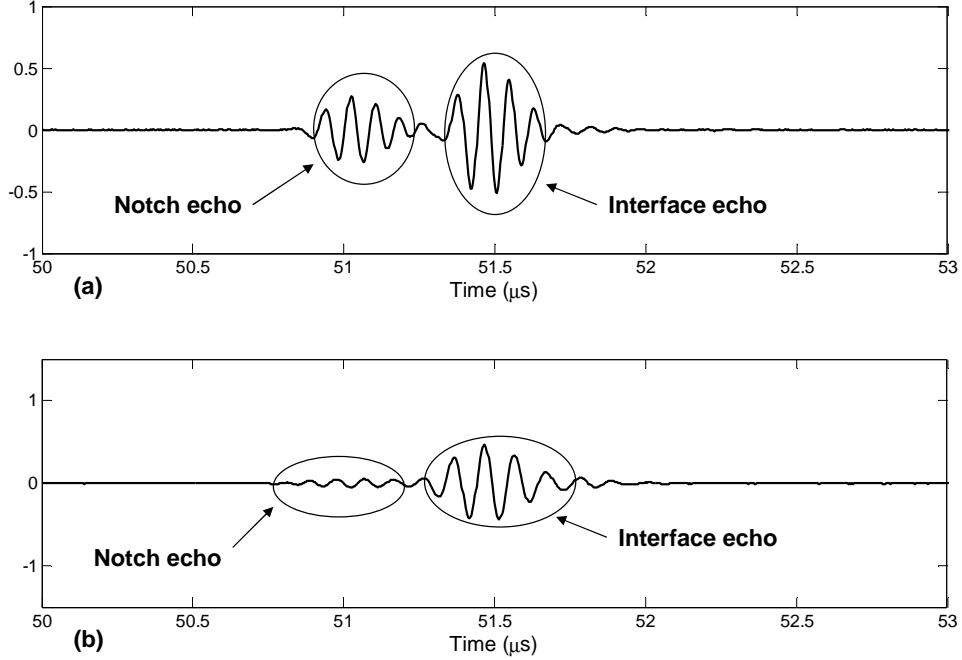


Figure 34: Pulse-echo waveforms in cylindrical waveguides of length 152.4 mm (6") (a) Rod of diameter 9.54 mm (3/8") with a notch of reflective area of 56% ($d_n=3.21$ mm). (b) Rod of diameter 12.7 mm (1/2") with a notch of reflective area of 33% ($d_n=1.73$ mm).

5.2 Measurement Methods

Chapter II introduced trailing echoes and their associated negative impact on thickness measurements. The implementation of waveguides thus needs to be studied carefully to enable thickness measurements.

5.2.1 Pulse-Echo Configuration

After the notch introduction, pulse-echo measurements consist in calculating the time delay between the notch echo and the backwall echo. Then the thickness is deduced

through

$$h_c = c_0 \frac{(\Delta t - t_0)}{2}, \quad (20)$$

where c_0 is the originally calibrated longitudinal wave speed, Δt is the time delay between the notch echo and the backwall echo, and t_0 is the initial calibration factor that includes the notch compensation.

However, the access to the arrival time of the backwall echo can be impeded by the trailing echoes associated with the calibration echo. Their attenuation is thus necessary to avoid these situations.

As suggested in chapter IV, the use of tapered rods can be a solution as they attenuate the trailing echoes. However, with the waveguide dimensions chosen, the efficiency of this solution is limited to the case when the transducer is in contact with the smaller end of the rod as illustrated on Figure 35.

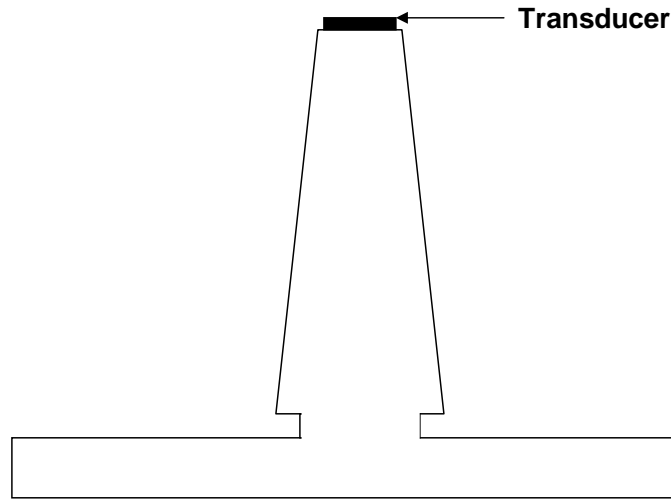


Figure 35: Pulse-echo measurements with a tapered rod.

An alternative solution is made possible by the welding operation. Without the notch, the reference echo and its associated trailing echoes would either not exist or be reduced in amplitude. It is thus possible to scale these echoes through notch

dimensioning. In particular, the trailing echo amplitudes can be chosen to be small in comparison with the amplitude of the backwall echo by reducing the notch depth. However, the notch echo also needs to be detectable. As a result, this solution is relevant only if the notch echo has a larger amplitude than its associated trailing echoes. The energy partition between these echoes depends on the dimensions of the rod. The adaptation of the waveguide to enable measurements is illustrated in Figure 36.

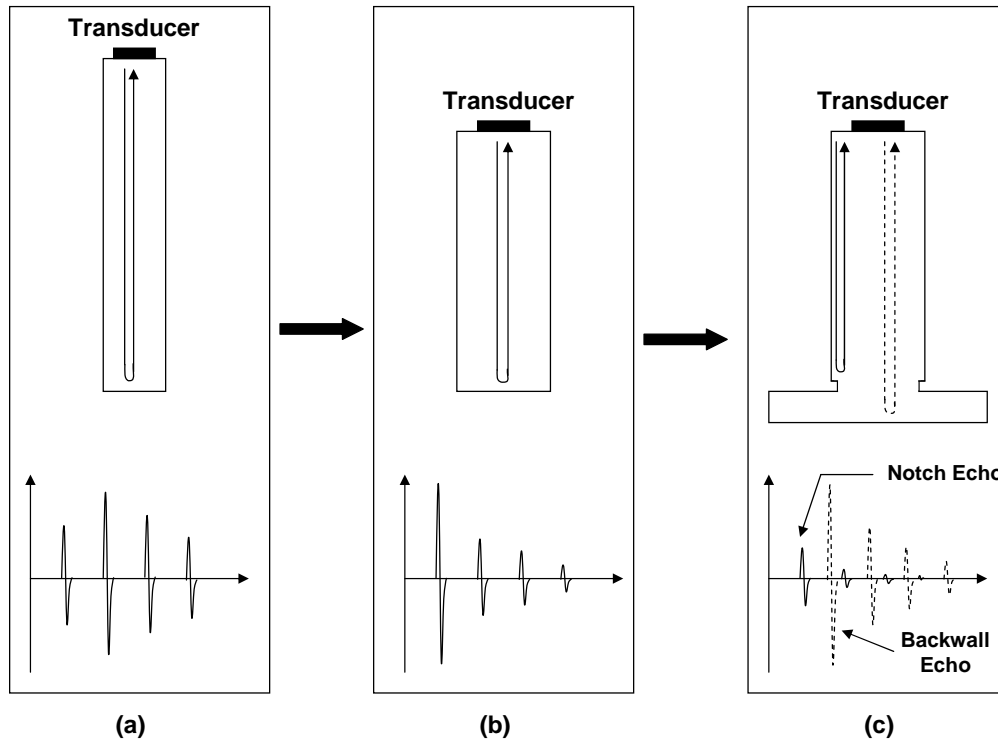


Figure 36: Design of a cylindrical waveguide enabling pulse-echo thickness measurements. (a) Random waveguide and its pulse-echo waveform. (b) Optimization of the rod dimensions for the first arrival to be more important than its trailing echoes. (c) Notch dimensioning to minimize the trailing echoes associated with the calibration echo while increasing the amplitude of the backwall echo.

However, with the waveguides chosen, the notch echo is not larger than its associated first trailing echo, and this solution is not implementable. In addition, measurements performed with welded waveguides showed a reflected echo coming back

from the weld, and this solution becomes irrelevant if the amplitude reflected from the weld is not small in comparison with that of the backwall echo.

To conclude, the implementation of pulse-echo measurements without modification of the waveguide's dimensions is limited to the use of a tapered rod in the configuration presented in Figure 35. If the rod's dimensions could be changed, more interesting solutions could be implemented.

5.2.2 Pitch-Catch Configuration

A pitch-catch configuration with a single waveguide is not a relevant option. Instead, pitch-catch measurements are performed with two distinct transducers, each mounted on a different waveguide as illustrated in Figure 37. The transmitter also operates in pulse-echo mode to receive the echo resulting from the wave reflection on the notch. The backwall echo is obtained from the through-transmission waveform. If the two waveguides are identical, the time-of-flight through the specimen can be determined by subtracting the arrival time of the notch echo from the arrival time of the backwall echo, which is essentially a mode 2 measurement. The angular path through the plate is then compensated via initial calibration and the thickness is determined as per Eq.(20).

This configuration presents a real advantage since it only uses first arrivals. The trailing echoes always arrive later than the first arrivals and they will no longer impede thickness measurements. The shape of the rods can thus be chosen arbitrarily as long as the energy transmitted through them is sufficient for the echoes of interest to be detected.

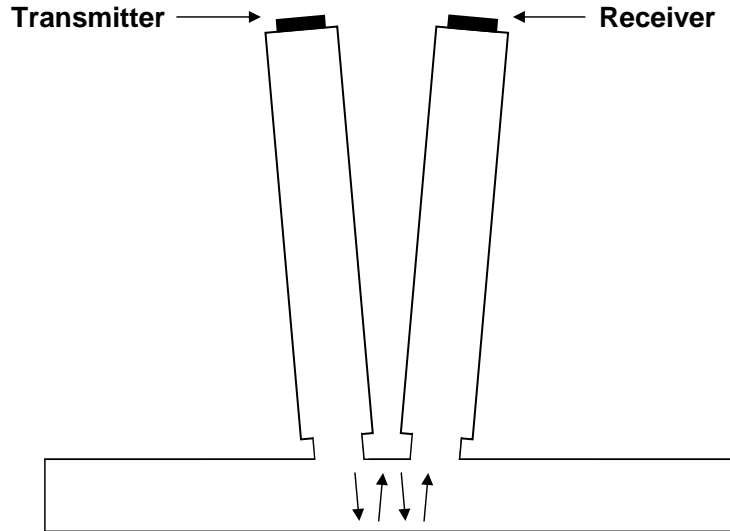


Figure 37: Thickness measurement in a pitch-catch configuration with waveguides.

5.3 Final Design

5.3.1 Discussion and Choice

Both pulse-echo and pitch-catch configurations can be implemented for thickness measurements with waveguides. However, they present different advantages and drawbacks that have to be considered for the choice of the final design.

Pulse-echo measurements are preferred as their welding is easier and because they divide the hardware price by a factor two. However, they are strongly dependant on the waveguide dimensions, which depend themselves on a set of external constraints. For the specific application considered here, the implementation of pulse-echo measurements is restricted to the configuration presented in Figure 35, where the transducer is mounted on the smaller diameter end. The heat transfer from the pipe to the transducer is then favored, which is not desired, and thus the pitch-catch configuration is chosen.

In the case when the thermal gradient inside the rod is not sufficient to guarantee the safety of the transducer and its coupling, it is envisioned to add heat sinks on the

waveguides. In this perspective, the use of tapered rods makes this operation more complex, and pitch-catch measurements with straight rods are preferred to pulse-echo measurements with tapered rods.

A later step consists of studying the propagation of waves in pipe walls to enable large area monitoring. In this perspective, the pitch-catch configuration may be more effective for sending waves into pipe walls. Finally, pitch-catch measurements are more robust to irregularities in the back surface of the pipe walls.

Depending on the dimensions of the monitored pipelines, it may be possible to modify the rod dimensions to enable effective implementation of pulse-echo measurements. However, the pitch-catch method is chosen for final implementation.

5.3.2 Concept Validation

Though theoretical studies are encouraging, they need to be confirmed experimentally. The pitch-catch configuration was thus implemented to prove the concept feasibility. Special holders needed to be designed for the proper insertion of waveguides during the welding operation. The time frame allocated to this thesis did not allow the machining of such holders, and experiments were performed with traditional coupling. In a pitch-catch configuration, measurements are based on first arrivals only, and are thus unaffected by any echo as from the weld interfaces. As a result, the use of traditional coupling is sufficient for concept verification.

Two cylindrical rods of length 152.4 mm (6") and diameter 9.54 mm (3/8") were machined with a notch of inner diameter 6.38 mm (1/4"). Their end was cut at an angle of 5 degrees to enable pitch-catch measurements. Then, a Plexiglas block was used to hold the rods in their intended positions. Panametrics couplant A was used to couple the rods to the plate and the transducers to the rods. The experimental setup is shown in Figure 38.

The pulse-echo and pitch-catch waveforms were then acquired and are presented

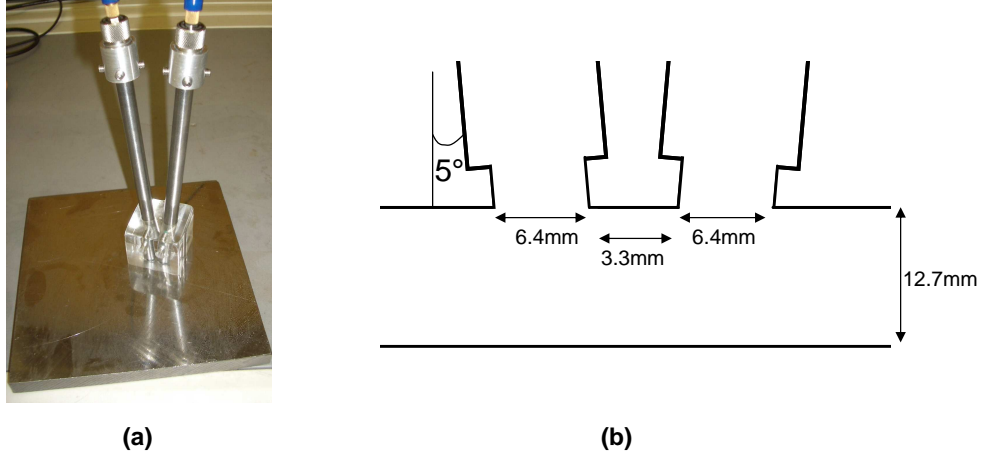


Figure 38: Experimental setup for concept verification of the pitch-catch measurements (a) Picture of the actual setup. (b) Parameters of the experiment.

in Figure 39. The two echoes of interest appeared clearly and their arrival times were determined for further analysis of the wave behavior.

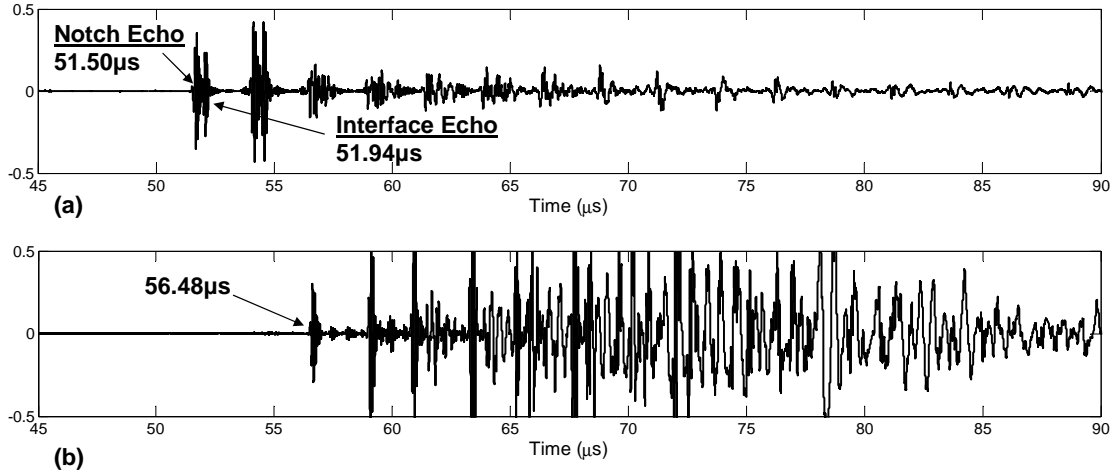


Figure 39: Experimental waveforms for pitch-catch measurements. (a) Pulse-echo waveform. (b) Through-transmission waveform.

Theoretical ray calculations based on waves entering the plate with a 5 degrees angle gives a W-path between the two waveguides, and the corresponding time of flight can be calculated as,

$$\Delta t = \frac{4d}{\cos(\theta)c_L}, \quad (21)$$

where d is the thickness of the plate, c_L is the longitudinal wave speed in steel, and θ is the angle of incidence of the wave into the plate. The short path in the ends of the rods is neglected. After replacement of each parameter by its value, a result of $8.79 \mu s$ is obtained.

Experimentally, the time-of-flight can be determined with the interface echo since the rods are not welded. The measured value is then $4.54 \mu s$. The difference from the calculation of Eq.(21) suggests the existence of a V-path through the plate rather than a W-path. It can be explained by the diverging waves as the sound enters the plate through the end of the rod.

Data were acquired from the experimental configuration of Figure 38, and time-of-flights for thicknesses of 12.7 mm (1/2"), 15.9 mm (5/8"), 19.05 mm (3/4"), and 25.4 mm (1") were measured and plotted against the corresponding thickness, along with the linear fit. The data confirms the validity of initial calibration in the range of thicknesses considered. The thickness is thus related to the time-of-flight through,

$$h_c = a_0 + a_1 \Delta t, \quad (22)$$

where a_0 and a_1 are calibration coefficients obtained through linear regression on the experimental data ($a_0=-2.11, a_1=2.97$).

Finally, the accuracy of measurements with temperature variations was verified and compared to the results obtained without on-line mode 2 compensation. The experimental setup was placed in an industrial oven and warmed to $42^\circ C$. Then, it was placed at room temperature, and measurements were performed as it cooled down. The value of the highest temperature for which measurements were performed was kept low, because the efficacy of waveguides in reducing the temperature still needs to be verified and cooling solutions such as the addition of heat sinks might be needed to avoid transducer damage.

Figure 41 compares the results of measurements with and without pulse-echo

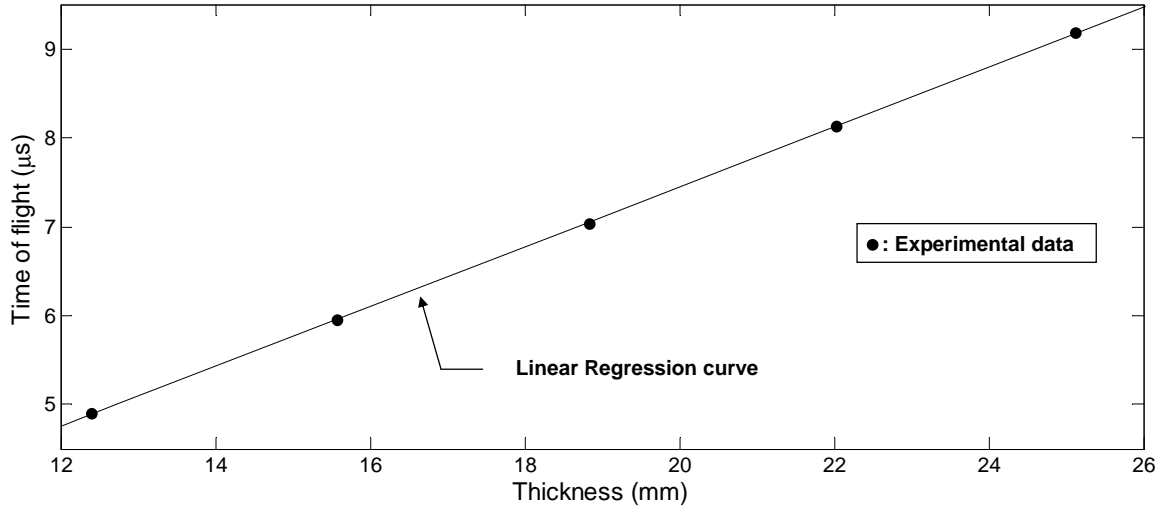


Figure 40: Generation of trailing echoes in a cylindrical waveguide.

compensation at room temperature (i.e. mode 2 vs mode 1). As expected, accurate results are obtained through both methods since the initial calibration was performed at room temperature.

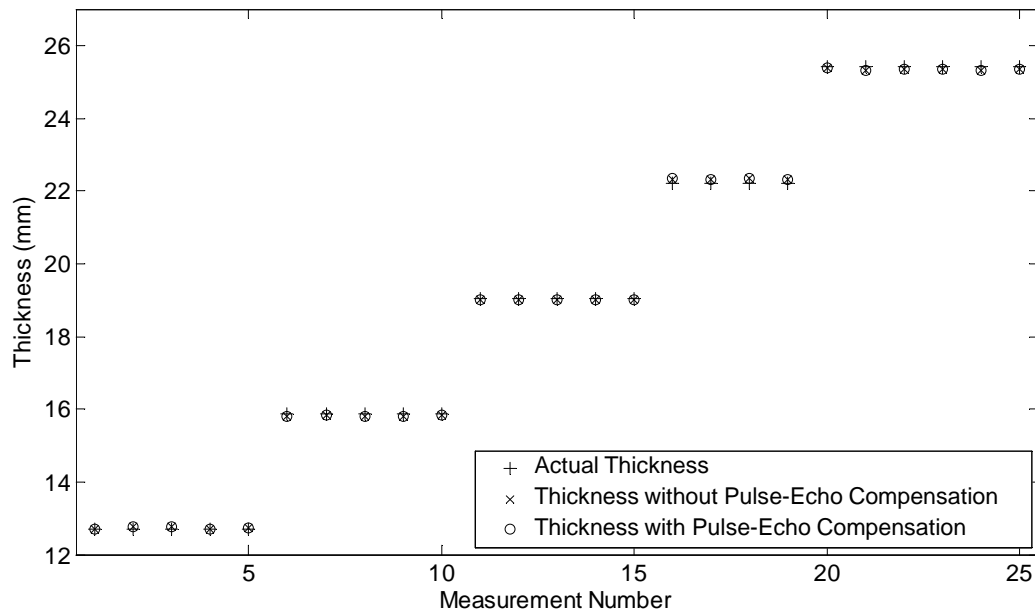


Figure 41: Thickness measurements at room temperature.

Figure 42 presents the evolution of the measured thickness at elevated temperatures. With pulse-echo compensation, the measurement error is small. Some errors

are caused by the hand coupling of the waveguides. However, as expected, a larger error is introduced without the pulse-echo compensation, which demonstrates the usefulness and efficacy of the proposed method.

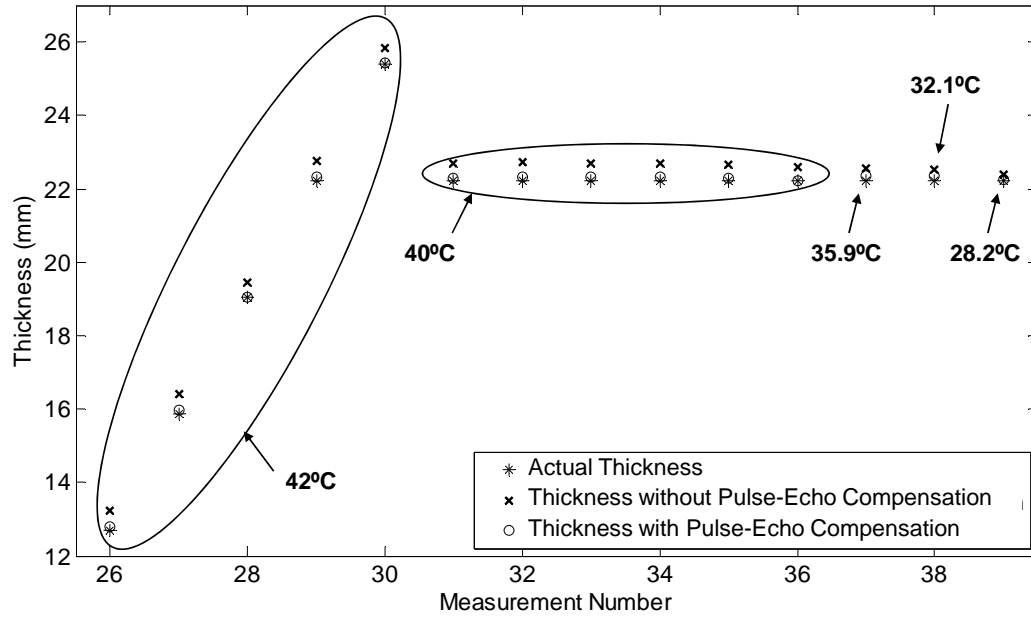


Figure 42: Results of thickness measurements at elevated temperatures. The initial calibration was performed at 22.5 °C.

CHAPTER VI

CONCLUSION

6.1 Summary and Conclusions

The objective of this thesis has been the development and verification of methods for on-line thickness monitoring of piping systems and pressure vessels at high temperature. The decision to use welded waveguides had already been made based upon prior work where multiple coupling methods were investigated [22], and thus the focus of this thesis has been the determination of the precise configuration to employ.

A study was performed to understand both pulse-echo and through-transmission wave propagation in straight and tapered buffer rods. The primary issue was generation of trailing echoes in such rods and their impact on thickness measurements. A prior literature search indicated that increasing the taper angle would reduce trailing echoes in long buffer rods. Experiments were performed, finite difference simulations were made, and a ray tracing model was developed to enable understanding of wave propagation in tapered buffer rods. It was found that the results for long buffer rods do not apply to shorter rods. Unlike reported results for longer rods, signals obtained with the transducer mounted on the larger end of a short tapered rod are significantly noisier in terms of trailing echoes than signals obtained with the transducer mounted on the other end. Although a modest taper angle does reduce the trailing echoes, further increases in taper angle do not provide additional improvement because the shorter length of the rod limits the number of mode conversions that can occur and thus limits the variability in the arrival times of different beam paths. The conclusion reached was that reasonable combinations of the diameter, length and taper angle of the buffer rod would not be adequate to reduce trailing echoes enough to permit

pulse-echo thickness measurements of pipe walls at high temperature.

A pitch-catch configuration was then considered using two adjacent buffer rods mounted at a small angle to the exposed surface. For this configuration, the backwall echo is the first arrival and is thus not affected by trailing echoes. The problem is that temperature-induced velocity changes cause time shifts in this arrival that could be mistaken for thickness changes. The proposed solution is to machine a notch in the rods close to their attachment points on the surface and to simultaneously record the pulse-echo signal. The arrival time of the echo reflected from the notch can then be used to compensate the error introduced by waveguides in the pitch-catch arrival time, thereby reducing the sensitivity of the thickness measurements to velocity perturbations. Measurements were performed to verify the efficacy of this proposed solution.

6.2 Future Work

It is critical that the proposed pitch-catch method be verified using welded rods at high-temperatures, and future work must include such experiments. The verification should include the accuracy and robustness of the ultrasonic method as well as thermal considerations. If the temperature at the transducer is too high to ensure survivability, then the waveguide will need to be cooled. The preferred method would be installation of passive heat sinks on the rods.

Once point thickness measurements are implemented, the ability to use the same rods and transducers to generate guided waves in the pipe walls should be investigated. The objective would be to enable large area monitoring between locations of point measurements.

Finally, further investigation of a pulse-echo solution should be considered. If the rod is made longer and the taper angle is increased, it may be possible to make thickness measurements. The primary issue would be whether the signal-to-noise

ratio of the backwall echo is sufficiently large.

REFERENCES

- [1] American Petroleum Institute. *Technology Vision 2020: A Technology Vision for the U.S Petroleum Refining Industry*, 1999.
- [2] D. E. Bray and R. K. Stanley. *Nondestructive Evaluation : A Tool in Design, Manufacturing, and Service*. CRC Press, 1997.
- [3] J. Krautkramer. *Ultrasonic Testing of Materials*. Springer, 1990.
- [4] C. R. Farrar and K. Worden. An introduction to structural health monitoring. *Phil. Trans. R. Soc. A*, 365:303–315, 2006.
- [5] M. Fields. Inservice pressure vessel inspections. *Proceedings of SPIE*, 3398:66–74, 1998.
- [6] K. A. Fowler, G. M. Elfbaum, K. A. Smith, and T. J. Nelligan. Theory and application of precision ultrasonic thickness gauging. *Insight - Non-Destructive Testing and Condition Monitoring*, 38(8):582–587, 1996.
- [7] Panametrics. *Panametrics-NDT Ultrasonic Transducers*, 2008. pp. 8-9.
- [8] A. E. H. Love. *The Mathematical Theory of Elasticity*. Cambridge University Press, London, fourth edition, 1934. p289.
- [9] H. J. McSkimin. Propagation of longitudinal waves and shear waves in cylindrical rods at high frequencies. *J. Acoust. Soc. Am.*, 28(3):484–493, 1956.
- [10] W. P. Mason and H. J. McSkimin. Attenuation and scattering of high-frequency sound waves in metals and glasses. *J. Acoust. Soc. Am.*, 19(3):464–473, 1947.
- [11] E. P. Papadakis. Buffer-rod system for ultrasonic attenuation measurements. *J. Acoust. Soc. Am.*, 44(5):1437–1441, 1968.
- [12] V. S. K. Prasad. Viscosity measurements of melts at high-temperatures using ultrasonic guided waves. *J. Material Processing Technology*, 207(1-3):315–320, 2008.
- [13] R. N. Thurston. Elastic waves in rods and clad rods. *J. Acoust. Soc. Am.*, 64(1):1–37, 1978.
- [14] H. J. McSkimin. Measurement of ultrasonic wave velocities and elastic moduli for small solid specimens at high-temperatures. *J. Acoust. Soc. Am.*, 31(3):287–295, 1959.

- [15] C.-K. Jen, L. Piche, and J. F. Bussiere. Long isotropic buffer rods. *J. Acoust. Soc. Am.*, 88(1):23–25, 1990.
- [16] C.-K. Jen, J.-G. Legoux, and L. Parent. Experimental evaluation of clad metallic buffer rods for high temperature ultrasonic measurements. *NDT&E International*, 33(3):145–153, 2000.
- [17] I. Ihara, D. Burhan, and H. Aso. Ultrasonic in-line sensors for inclusion detection in liquid metals. *IEEE Ultrasonics Symposium*, 1:811–814, 2002.
- [18] Y. Ono, J.-F. Moisan, and C.-K. Jen. Ultrasonic techniques for imaging and measurements in molten aluminum. *IEEE Trans. Ultrason., Ferroelect. Freq. Contr.*, 50(12):1711–1721, 2003.
- [19] L. C. Lynnworth, Y. Liu, and J. A. Umina. Extensional bundle waveguide techniques for measuring flow of hot fluids. *IEEE Trans. Ultrason., Ferroelect. Freq. Contr.*, 52(4):538–543, 2005.
- [20] Piezotechnologies. High temperature transducers. <http://www.piezotechnologies.com/temp900.htm> (Last visit 12 November 2008).
- [21] S. P. Kelly, I. Atkinson, G. Chris, and K. J. Kirk. On-line ultrasonic inspection at elevated temperatures. *IEEE Ultrason. Symp.*, pages 904–908, 2007.
- [22] Mechanical Integrity, Inc. Private communication with Donald McNicol.
- [23] Cyberlogic, Inc. Wave2000 Software for Computational Ultrasonics. www.cyberlogic.org/wave2000.html (Last visit 12 november 2008).
- [24] J. A. Johnson, N. M. Carlson, and L. A. Lott. Ultrasonic wave propagation in temperature gradients. *J. NDT&E*, 6(3):147–157, 1987.
- [25] J. D. Achenbach. *Wave Propagation in Elastic Solids*. North-Holland, New York, 1999.
- [26] Panametrics. *Ultrasonic Transducers Technical Notes*, 2006. p 43.
- [27] B. A. Auld. *Acoustic Fields and Waves in Solids*. Robert E. Krieger Publishing Company, Inc., 2nd edition, 1990.
- [28] G. Mott. Temperature dependence of ultrasonic parameters. *Review of progress in Quantitative Nondestructive Evaluation*, 3B:1137–1148, 1984.
- [29] C. E. Jaske, J. A. Beavers, and N. G. Thompson. Improving plant reliability through corrosion monitoring. In *Proceedings of the Fourth International Conference on Process Plant Reliability*, pages 3–18, Houston, TX, 1995.